Chapter 7. Direct Synthesis and Mechanism for the Formation of Mixed Metal Fe_2Ni-MIL-88B

Gia-Thanh Vuong, Minh-Hao Pham and Trong-On Do *

Department of Chemical Engineering, Laval University, Quebec G1K 7P4, Canada

Submitted to CrystEngComm 2013.

Résumé

Le mécanisme de synthèse a été étudié pour la synthèse Fe_3-MIL88B et Fe_2Ni-MIL88B. Ces matériaux ont été caractérisés par différentes techniques, telles que la spectroscopie UV-Vis, IR et Raman et la diffraction des RX. Les résultats montrent que pour la synthèse de Fe_3-MIL88B, le mono-métal Fe_3-MOF-235 se forme en première étape de synthèse et joue le rôle de précurseur (germe) pour la formation de Fe_3-MIL-88B: les germes MOF-235 sont formés, ensuit se transforment en Fe_3-MIL-88B. Dans le cas d'utilisation du cluster de métaux mixtes $Fe_2Ni(\mu_3\text{-}O)$, les mono-métaux Fe_3-MOF-235 formés en premier étape jouent le rôle comme germes pour la croissance de matériau Fe_2Ni-MIL88B. L'anion $FeCl_4^-$ est très important pour le succès de la formation de MOF-235. Un mécanisme d'anion médiateur dans la formation de MOF-235 a été suggéré.

Abstract

The direct synthesis of Fe_3-MIL-88B and Fe_2Ni-MIL-88B was analyzed using different characterization techniques including UV-Vis, IR, Raman spectroscopies and XRD. It was found that single metal Fe_3-MOF-235 seeds which were formed from the first stage of synthesis are as precursors for the formation of MIL-88B. Fe_3-MOF-235 seeds formed in the first stage of synthesis were then transformed to Fe_3-MIL-88B in the case of single metal, and to mixed Fe_2Ni-MIL88B in the case of mixed metal synthesis. In the both cases of Fe_3-MIL-88B and Fe_2Ni-MIL-88B, $FeCl_4^-$ anion is a key feature to the formation of MOF-235. An anion mediated mechanism for the formation of MOF-235 structure is also suggested.

7.1. Introduction

Metal-organic frameworks (MOFs) are one of the fastest growing fields of chemistry.[1] The structure of MOFs is formed by a polymeric connection of a metal cluster in coordination bond with an organic linker, which results in a vast collection of MOFs.[2] As a typical MOF structure, MIL-88B is of special interest due to its potentials in adsorption, catalysis, biomedicine.[3-7] Its structure is built on the connection of 1,4-bezenedicarboxylate (bdc) with trinuclear oxo-centered metal cluster (Me_3O, Me = Fe, Cr, Sc). Several trinuclear metal clusters have been reported in successful synthesis of MIL-88B yielding Fe_3-MIL-88B, Cr_3-MIL-88B and Sc_3-MIL88B.[6, 8, 9] In our recent publication,[10] a novel route to prepare a new type of mixed metal MIL-88B structure was reported. Unlike the conventional negative charged single metal cluster, the use of neutral mixed metal cluster as nodes in the framework avoids the need of compensating anion inside porous MIL-88B system. As a result, this mixed metal MIL-88B becomes porous. Furthermore, the flexibility of the mixed metal MIL-88B can be controlled by terminal ligands with different steric hindrance. This allows us to reversibly customize the porosity of MIL-88B structure at three levels of specific surface area as well as the pore volume.[10]

In the synthesis of trinuclear-based MOFs such as MIL-88B and MIL-101, when iron and 1,4-bezenedicarboxylic acid (bdc) are used in the presence of DMF, the kinetically and thermodynamically stable phases are MIL-88B and MIL-101 which form at low temperatures (≤100 °C), and thermodynamically stable MIL-53, which forms at higher.[11, 12] When a second metal is introduced in the reaction medium to obtain the mixed metal MOF, the situation becomes more complicated. There are competing reactions to yield single metal and mixed metal MOFs. It is also necessary to determine which factors promote the single metal MOF and which factors promote the mixed metal MOFs and why. A detailed study of the synthesis of both the single metal and mixed metal of trinuclear based MOF could contribute to the understanding of the kinetics and mechanism of the MOF formation

In this study, as the continuing part of the previous publication,[10] we report the effect of several factors on the formation of both single metal Fe_3-MIL-88B and mixed metal Fe_2Ni-MIL-88B. It occurred to us that even though the synthesis of mixed metal

MOFs is more complicated than that of the single metal one, the presence of the second metal was found to be helpful in determination of the important initial solid Fe_3-MOF-235, revealing a vital template effect from a surprising source: halogen anion. The impacts of pH, concentration, second metal were considered and illustrated. We also found similarities in the principles of synthesis between zeolites and MOFs, which can be used as a guideline for the synthesis of porous materials.

7.2. Experimental Section

Chemicals: $FeCl_3.6H_2O$ (99%) and $Fe(NO_3)_3.9H_2O$ (98%), 1,4-bezenedicarboxylic acid (bdc, 98%), NaOH (99%), N,N-dimethyl-formamide (DMF) were used as purchased.

Synthesis: Syntheses of Fe_3-MIL-88B and Fe_2Ni-MIL-88B were carried out following our previous work.[10] Two series of samples with different times of crystallization were prepared using two different iron sources, $FeCl_3.6H_2O$ and $Fe(NO_3)_3.9H_2O$: single metal and mixed metal based MIL-88B. (i) For single metal based MIL-88B synthesis: 5 vials of 10 ml DMF solution containing 10 mmol of $FeCl_3.6H_2O$ 99% (or $Fe(NO_3)_3.9H_2O$ 98%) was added with 10 mmol 1,4-bezenedicarboxylic acid (bdc) under stirring at room temperature. Subsequently, 4 ml of NaOH 2M was rapidly injected under continuous stirring. The vials were then capped and heated at 100 ^oC for different times: 0 h (e.g., 5 min after the addition of NaOH at room temperature), 1h, 2h, 3h, and 12 h. (ii) For mixed metal based MIL-88B synthesis: the same procedure was also applied for the synthesis of mixed metal MIL-88B, except that 10 ml DMF solution containing 3.33 mmol of $Ni(NO_3)_2.6H_2O$ and 6.67 mmol of $FeCl_3.6H_2O$ 99% (or $Fe(NO_3)_3.9H_2O$ 98%) were used. Solids products were recovered by centrifugation at 5000 rpm for 5 min. The solids were then dried in vacuum for 24 h at 50 ^oC. In general, the samples prepared with $FeCl_3.6H_2O$ yield firm solids. However, those prepared from $Fe(NO_3)_3.9H_2O$ become thick gel during the heat treatment and thus, their corresponding solid products are not as firm as the solids prepared from $FeCl_3.6H_2O$. The samples are designated as [Metal cluster]-[Anion type]-[Synthesis time]. For example, Fe_2Ni-Cl-5h is the mixed metal MIL-88B sample prepared at 100 ^oC for 5 h using $FeCl_3 \cdot 6H_2O$.

Characterization Methods: FTIR was carried in a FT-BIORAD 450s instrument using KBr disc. FTIR spectra were normalized by setting the transmittance value of the band at 750 cm^{-1} which represents the strong vibration of the C-H bond to 0.05. UV-Vis analysis was carried out in a Cary 300 instrument using MgO disc as the reference sample. Normalization of the spectra was done by setting the value of the strongest absorbance band at 350 nm to 1. Raman analysis was carried out with a Horiba U100 Raman spectrometer using excitation wavelength of 514 nm. The spectra were normalized by setting the value of the strong absorbance band of the benzene ring at 1615 cm^{-1} to 1. Powder X-ray diffraction (XRD) patterns were collected on a Bruker SMART APEX II X-ray diffractometer with Cu Kα radiation (λ = 1.5406 Å) in the 2θ range of 1 - 20° at a scan rate of 1.0° min^{-1}. HRTEM analysis was carried out with a Hitachi HF-2000 Field Emission TEM. EDS analysis was done with a fine electron probe of 3 nm, the acquiring time was set to 200 sec. Samples were dispersed on a copper grid.

7.3. Results

UV-Vis spectra: UV-Vis spectra of the two series of single metal and mixed metal based samples are shown in Figure 7.1 and Figure 7.2. For the single metal synthesis, the UV-Vis spectra of the samples do not change much over the synthesis times; it is likely that the Fe^{3+} species (octahedral configuration) remains the same throughout the synthesis. For the mixed metal samples, most of the transition bands of Ni^{2+} are obscured or overlapped by those of Fe^{3+}, however, the presence of octahedral Fe^{3+} is verified. The transition [$^6A_{1g}$ => $^4A_{1g}$ + $^4Eg(G)$] in Fe^{3+} is found at 350 - 500 nm and the [$^6A_{1g}$ => $^4T_{2g}$] transition at 550 - 650 nm is also attributed to Fe^{3+}.[13, 14] In contrast to the single metal, the UV-Vis spectra of the mixed metal samples change considerably with the synthesis time. In the Fe_2Ni complex under the effect of Ni,[13] the ligand field in Fe reduces, thus the [$^6A_{1g}$ => $^4T_{2g}$] transition in single metal samples (Fe_3O) is at 525 nm while it is observed at 575 nm in the Fe_2Ni. In the spectra of mixed metal Fe_2Ni-MIL-88B, the band at 760 nm is observed. This band is characteristic of the transition [$^3A_{2g}$ => $^1E_g(D)$] of Ni in the tri-nuclear cluster [13] and thus it can be used as an indicator of the formation of the mixed metal cluster Fe_2NiO. The evolution of the UV-Vis spectra over synthesis time of both syntheses using $Fe(NO_3)_3.9H_2O$ and $FeCl_3.6H_2O$ exhibits a similar trend. At 0 h, the spectra

are similar to the single metal samples; no band at 760 nm is observed. However after 3 h, the band 760 nm is found in two series of mixed metal samples prepared using $Fe(NO_3)_3.9H_2O$ and $FeCl_3.6H_2O$, the intensity of this band increases with synthesis time, up to 12 h (Fig. 2). This suggests that at the early stage of synthesis, only Fe^{3+} is present in the solid, and after that the mixed metal cluster Fe_2Ni is formed. In other words, the formation of Fe_3O cluster takes place first, followed by that of the mixed metal cluster Fe_2NiO. The difference between the mixed metal syntheses using $Fe(NO_3)_3.9H_2O$ and $FeCl_3.6H_2O$ is the rate of the formation of Fe_2NiO cluster. For the sample prepared using $Fe(NO_3)_3.9H_2O$, the band at 760 nm is very weak even after 12 h of synthesis; however, for the sample prepared using $FeCl_3.6H_2O$, this band is readily observed after only 2 h of synthesis and it still remains its strong intensity after 12 h (Figure 7.2).

FT-IR spectra: The FTIR band at 1660 cm^{-1} which is characteristic of DMF was observed on all of the samples (Supporting information), as also reported in ref [15]. The presence of free bdc linker (FTIR band at 1700 cm^{-1}) [16] was observed on the samples prepared from $Fe(NO_3)_3.9H_2O$ but not on those prepared from $FeCl_3.6H_2O$. This absence of free acid bdc in the Cl^- based samples is interesting given the fact that no effort was made to wash the obtained solid off free bdc acid. This observation implies that under these investigated conditions; H_2BDC is mostly deprotonated when Cl^- is used. The free bdc observed in the NO_3^- based samples also relates to its gel-like behavior of the products while the Cl^- based synthesis produces firmly solid products.

Detailed analysis was focused on the wavelength range from 400 – 800 cm^{-1} which includes the well-documented framework vibration of the trinuclear cluster.[17, 18] The FTIR band assignments in this range are showed in Table 7.1. Beside the presence of the vibrations of the organic ligand bdc, the vibration of the central oxygen in single Fe_3O and mixed Fe_2NiO clusters at 720 and 620 cm^{-1} was observed, respectively. Since the central oxygen is available only in the trinuclear clusters, these FTIR bands are considered as their indicators. And the presence of Fe_3O and Fe_2NiO can be distinguished.

For the single metal samples at different synthesis times, only the Fe_3O vibration (600 – 625 cm^{-1}) which is of interest is shown in Figure 7.3. The vibration of Fe_3O is observed in all the samples. The band is well defined at synthesis time 0 h and continues to

remain strong at the synthesis time 12 h. This implies that the cluster Fe_3O is formed fast and remains stable under the synthesis conditions. For the samples that employ Cl^-, the FTIR band characterisric of Fe_3O is more intense and well-defined than those using NO_3^-.

The FT-IR spectra of the mixed metal samples are shown in Figure 7.4. The spectra exhibit a gradual development of Fe_2NiO clusters, and concomitantly with a decrease of Fe_3O ones. For the samples using Cl^-, at 0 h, (Figure 7.4B) after the addition of NaOH at room temperature, the FTIR band of Fe_3O was visible, while the band of Fe_2NiO was not found. However, after 1h, the FTIR band of Fe_2NiO was observed and the one of Fe_3O decreased. At 2 h and 3 h, the FTIR band of Fe_2NiO is prominent while that of Fe_3O becomes very weak. Finally after 12 h, only the well-defined band Fe_2NiO was observed while the band of Fe_3O almost disappeared. For the samples using NO_3^- (Figure 7.4A), the same trend was also observed. The FTIR band of Fe_3O appears first right at 0 h and decreases with the synthesis time. In contrast, the band of Fe_2NiO was observed only after 3 h. Thus, using $Fe(NO_3)_3.9H_2O$, the formation of Fe_2NiO clusters is much slower than that using $FeCl_3.6H_2O$. After 12 h, both FTIR bands of Fe_3O and Fe_2NiO were still observed.

In short, FTIR analysis of the mixed metal synthesis using NO_3^- (e.g., $Fe(NO_3)_3.9H_2O$) or Cl^- (e.g., $FeCl_3.6H_2O$) shows that both Fe_3O and Fe_2NiO clusters were produced, first Fe_3O then followed by Fe_2NiO. For the mixed metal synthesis using Cl^-, with increasing synthesis time, the Fe_2NiO cluster becomes the main one, while the Fe_3O cluster diminishes. In contrast, for the mixed metal synthesis using NO_3^-, both types of the clusters are observed at the end of the synthesis.

Raman spectra: The similar results were also observed for the Raman spectra. The bdc linker was found on all of the samples. The band at 631 cm^{-1} is assigned to the in-plane bending of the carboxylate group OCO.[19-21] The weak band at 1125 cm^{-1} is attributed to the vibration of C-COO.[22] The benzene ring in bdc gives rise to the vibrations at 860, 1146 and 11616 cm^{-1}. [19-21] The Raman spectra also reveal some key inorganic components in the samples. The vibrations of the trinuclear cluster are found at two weak bands 175 and 267 cm^{-1}.[23] The medium band at 430 cm^{-1} is assigned to the metal oxygen bond.[17] The bands at around 567cm^{-1} found only on the mixed metal samples are tentatively assigned to the asymmetric stretching mode of Fe_2NiO cluster.[19-21]

However, the most interesting results in the Raman analysis are the determination of the compensating anions for the Fe_3O cluster, e.g. NO_3^- and $FeCl_4^-$. As discussed earlier, for the single metal Fe_3O-based material, each Fe_3O carboxylate cluster in the framework needs an anion to balance the charge. A presence of Fe_3O clusters in the framework implies the necessary accompany of these anions. For synthesis using $Fe(NO_3)_3.9H_2O$, nitrate is likely the only anion available.

For the mixed metal syntheses using $FeCl_3.6H_2O$, beside the available nitrate which comes from $Ni(NO_3)_2$, the source of anions can also include Cl^- and $FeCl_4^-$. Although it is impossible to determine Cl^- in Raman spectra, the detection of $FeCl_4^-$ and NO_3^- is feasible.[17] The stretching vibration of $FeCl_4^-$ leads to a well-defined band at 330 cm^{-1}.[17, 24, 25] For NO_3^-, the symmetric N-O stretching vibrations give rise to the strong band at 1044 cm^{-1}. [17, 26, 27] Details of the band assignments are listed in Table 2. For the single and mixed metal syntheses using $Fe(NO_3)_3.9H_2O$ thus having only NO_3^- as the anion source, the presence of nitrate is found on all the samples, as observed by the Raman band at 1044 cm^{-1}. Nitrate anion content correlates well with Fe_3O clusters in the framework by the intensity of this Raman band at1044 cm^{-1} (Figure 7.6A). In the single metal synthesis, the band 1044 cm^{-1} of nitrate remains stable, in correlation with the readily formed Fe_3O clusters (Figure 7.5A). In the mixed metal synthesis using $Fe(NO_3)_3.9H_2O$, the band 1044 cm^{-1} grows in strength and shape over the synthesis time, implying an increase of the single metal cluster Fe_3O (Figure 7.6A). Taking into account of the FTIR spectra results, it suggests that although there is a competition from the formation of Fe_2NiO, the formation of the Fe_3O cluster is still favored when $Fe(NO_3)_3.9H_2O$ is used. In the mixed metal syntheses using $FeCl_3.6H_2O$, Raman spectra (Figure 7.6B) shows the presence of anion $FeCl_4^-$ by the Raman band at 330 cm^{-1}, which diminished during the synthesis; however, there is no nitrate found in the sample, this fact implies the high selectivity of $FeCl_4^-$ and Cl^- anions over NO_3^- of the clusters. In the single metal synthesis, $FeCl_4^-$ is found right at 0 h, however the Raman band at 330 cm^{-1} of $FeCl_4^-$ decreases sharply during the synthesis, after 3 h, this band of $FeCl_4^-$ is vanished (Figure 7.5B). It is likely that $FeCl_4^-$ decomposes, providing additional iron source for the growing Fe_3O clusters and leaving Cl^- as the balancing anion in the cluster. In the mixed metal synthesis using $FeCl_3.6H_2O$, this Raman band of $FeCl_4^-$ at 330 cm^{-1} is much smaller. Also the

decomposition of $FeCl_4^-$ is much faster, after 2 h, no significant band of $FeCl_4^-$ was observed, implying the formation of mixed metal cluster readily dominates and no compensating anion is needed as compared to that of the single metal one.

Thus, the spectroscopy data have allowed us to determine and distinguish Fe_3O and Fe_2NiO clusters as well as the balancing anions that accompany the formation of Fe_3O clusters. The results from the spectroscopy analysis suggest that: (i) in the single metal synthesis, Fe_3O clusters as nodes in the MOF structure were formed, regardless of anion used; (ii) in the mixed metal syntheses, when Cl^- was used in the synthesis mixture, single Fe_3O clusters were formed at the first stage, followed by the formation of mixed metal Fe_2NiO in the framework, which subsequently becomes the main clusters with increasing the synthesis time. At the initial stage, $FeCl_4^-$ is the main balancing anion for the Fe_3O clusters in the framework. It is then decomposed. Finally, the Cl^- becomes the balancing anion for the Fe_3O cluster. When NO_3^- was used, both Fe_2NiO and Fe_3O clusters were produced, however, free bdc was found. Trinuclear Fe_3O cluster exhibits high preference of Cl^- based anion ($FeCl_4^-$ or Cl^-) as balancing anion over NO_3^-. It is however noted that the spectroscopy data cannot reveal how the nodes and linkers arrange in space, in other words, they cannot confirm the crystalline or amorphous structure of the solids. To determine the structure and phase, the XRD analysis is needed.

XRD analysis: XRD patterns of the Fe_3- NO_3-x (A) and Fe_3-Cl-x (B) samples as a function of synthesis time are shown in Figure 7.7. The results revealed that, for single metal syntheses at 100 ^oC, the use of NO_3^- as anion in the synthesis mixture yields no definitive structure even after 12 h of synthesis, while using Cl^-, the Fe_3-Cl-x sample exhibits a gradual structure change from MOF-235 to MIL-88B as a function of synthesis time. As seen in Figure 7.7B, the solid obtained right after the addition of NaOH (at 0 h) exhibits readily the XRD pattern of the MOF-325 structure. And then in the next three hours at 100 ^oC, its XRD pattern is much more intense implying the increase of its crystallinity; and only MOF-235 phase was observed. However after 12 hours at 100 ^oC, the XRD pattern shows a mixture of both MIL-88B and MOF-235.

The similar trend is also observed for the synthesis of mixed metal MIL-88B (Figure 8). Again, Fe_2Ni-NO_3-x samples show essentially noncrystalline phase regardless

of the synthesis time (Figure 8A). In contrast, the sample Fe_2Ni-Cl-x clearly exhibits faster phase transition than the single metal synthesis. At 0 h after the addition of NaOH, although the MOF-235 phase was dominant, the MIL-88B was observed with the presence of weak peaks of the plane (101) and (002) (Figure 8B). After 1 h, the MIL-88B structure was established as the prominent and characteristic planes (100) (101) (002) appeared. However, the MOF-235 phase is still pronounced as its (101) plane is still intense. After 3 h, the MIL-88B phase became the major phase over the MOF-235 phase. The peaks characteristic of MOF-235 phase were very weak or disappeared. Eventually after 12 h, only MIL-88B in open form is present. Hence, the transformation from MOF-235 to MIL-88B in the mixed metal synthesis is faster than that of the single metal synthesis.

High-resolution transmission electron microscopy (HRTEM) and energy-dispersive X-ray spectroscopy (EDS) analysis: Other important information is whether the Fe/Ni ratio varies along its crystal. For this purpose, HRTEM and EDS techniques were employed; different Fe_2Ni-Cl-12h crystals were observed. A representative HRTEM image of a crystal of Fe_2Ni-Cl-12h sample is shown in Figure 7.9. The crystal is an elongated hexagonal bipyramid, which is 500 nm long and 80 nm wide. This crystal shape is frequently encountered for MIL-88B.[28, 29] EDS spectra were acquired on a large number of positions in the crystal. For example, as shown in Figure 7.9, a selection of 5 different positions are shown, they are two positions (1 and 4) near the external part of the crystal and three positions (2, 3 and 5) approaching the crystal center. The atomic ratios of Fe and Ni from the EDS spectra are also displayed in

Table 7.3. The results exhibit that the Fe/Ni ratio is not identical but does vary throughout the crystal. In terms of Fe/Ni ratio, the crystal is rich in Fe in the center but Ni content increases as one move outward. At the outer part of the crystal, the Fe/Ni reaches the value of 2, in agreement with the stoichiometric ratio of Fe_2NiO cluster. This behavior implies that the Fe_2Ni-MIL-88B crystal indeed includes both Fe_3O and Fe_2NiO clusters in the framework.

7.4. Discussion

General remarks: The phase selection and transition in the synthesis of MIL materials have been investigated by several groups.[30-33] The first report on this matter by Férey et al.[32] dealt with the synthesis of Fe based MIL-53 using dimeric metal cluster as its framework nodes. The authors found that, MOF-235 is formed at the first stage of synthesis, followed by the formation of MIL-53 product. As the SBUs of MIL-53 and MOF-235 are different, it would be impossible for a solid phase transition from MOF-235 to MIL-53. It suggests that during the MIL-53 synthesis, MOF-235 dissolves releasing free monomers to yield subsequent MIL-53. For the synthesis Cr-based MIL-53, Jhung et al.[30, 31] reported that MIL-101, but not MOF-235 is the transient phase and is subsequently converted into MIL-53 under the studied synthetic conditions. Recently, Stavitski et al. [33] studied on the synthesis of MOFs based on tri-nuclear cluster of Al, the authors' findings are in agreement with the previous reports by Férey and Jhung groups. In fact, they also suggest that MOF-235 is the first to appear and then forms the MIL-101, and finally they dissolve to yield MIL-53. Thus regardless of the metal cluster, a general rule is observed: MOF-235, which is kinetically favored, will be appeared first and play as the precursor to form MIL-101. Finally the most thermodynamically stable MIL-53 is formed at the expense of both MIL-101 and MOF-235. And as MIL-101 and MOF-235 are built on the same trinuclear cluster while MIL-53 employs the dimeric oxo-cluster, it is likely that trinuclear cluster is kinetically favored over dimeric one, however, tri-nuclear cluster is thermodynamically less stable than the dimeric one. To the best of our knowledge, no information about the phase transformation and the formation MIL-88B during the synthesis has been reported. Table 7.4 summarizes the crystal parameters of MIL-88B and MOF-235. For single metal Fe, both MOF-235 and MIL-88B structures are cationic framework of the same formula $Fe_3O(bdc)_3$. The difference in terms of composition is the compensating anions which are Cl^- in the MIL-88B and $FeCl_4^-$ in MOF-235. In regard to topology, MOF-235 and MIL-88B are identical; they are both built on the **acs** net,[34] having the same crystal and space group. In addition, thanks to the breathing capacity,[35] the a lattice constant can increase from 11 Å to 14 Å, while the c constant decreases from 19 Å to 14 Å, accordingly. This flexible range of lattice constant of MIL-88B structure comprehensively encompasses the lattice parameters of MOF-235. Hence topologically

speaking, structures of MIL-88B and MOF-235 are likely to be inter-convertible; one could be converted to other by distortion without breaking the linker bdc and the tri-nuclear cluster. And with this high similarity in structure of MIL-88B and MOF-235, it is likely that MIL-88B would form fast at initial stages, but does it come before or after MOF-235? In our study of the MIL-88B synthesis, a secondary metal (Ni) which can form stable mixed metal complex with Fe, is introduced, the situation would become more complicated, there would be the additional competition between mixed metal MIL and single metal MIL. However, as it will be explained later, the secondary metal Ni turns out to be useful, playing a role of spectroscopically labeled atom in the detection and distinction of single and mixed trinuclear clusters and thus it is possible to distinguish MOF-235 and MIL-88B structures.

Determination of phase transformation during the synthesis: As seen above in the FTIR, Raman and UV-Vis spectroscopy analyses, all the syntheses at first produce single metal solid (Fe) even in the case with the presence of secondary metal Ni. FTIR spectra of the solids also revealed the tri-nuclear Fe_3O cluster which is the building unit of MOF-235 and MIL-88B. However, based on the XRD results, these initial solids exhibit that only those prepared using the $FeCl_3.6H_2O$ source are structural and were identified as MOF-235, while no structural products were observed using $Fe(NO_3)_3.9H_2O$ as the Fe source during the synthesis. Furthermore, for the Cl^- based samples, the solid structure gradually changes from MOF-235 to MIL-88B with increasing the synthesis time. Along with this phase transformation, for the mixed metal synthesis, the mixed metal tri-nuclear cluster Fe_2NiO begins to appear. As seen in the FTIR spectra (Figure 7.4), the vibration of mixed metal cluster becomes pronounced over the synthesis time, while the vibration of single metal cluster diminishes. This accompanies with the decrease of $FeCl_4^-$ anions as shown in Raman spectra (Figure 7.6). Hence, the trend observed for the samples using $FeCl_3.6H_2O$ is as follows: MOF-235 comes first, and then MIL-88B which is more stable comes later and gradually takes over the MOF-235. The MIL-88B develops thanks to the transformation from the MOF-235 structure. The phase transformation from MOF-235 to MIL-88B is also observed and is found to be fast. In addition, there are competing reactions forming Fe_3-MIL-88B and Fe_2Ni-MIL-88B. The formation of single metal cluster Fe_3O dominates at the initial stages with the formation of MIL-235, and then Fe_3-MIL-88B.

Subsequently, it is surpassed by the formation of mixed metal cluster Fe_2NiO for the Fe_2Ni-MIL-88B synthesis. However, this behavior is not observed for the mixed metal synthesis using $Fe(NO_3)_3.9H_2O$. No MOF-235 was produced during the synthesis; especially, amorphous solid product was yielded. Strictly speaking, Cl^- is required in composition of MOF-235. This also implies that MOF-235 would play an important role for the phase transformation from MOF-235 to MIL-88B.

The HRTEM and EDS analyses show that in the mixed metal synthesis using Cl^-, the Fe_3 and Fe_2NiO clusters are not distributed separately in two kinds of crystals Fe_3-MIL-88B and Fe_2Ni-MIL-88B, respectively. In fact these clusters reside in the same crystal in which the Fe_3O cluster prefers the center while the Fe_2Ni ones take the outward place. Taking into account the findings of the spectroscopy data and XRD analysis, it is suggested that, the formation of Fe_2Ni-MIL-88B at first starts with single Fe_3O cluster in form of MOF-235 and then Fe_2NiO cluster comes in as the crystal grows. The kinetically favored MOF-235 could be seeds or in other word precursors to subsequent growing of thermodynamically stable MIL-88B structure. Without MOF-235, the formation of the coordination framework is much more difficult as in the case of nitrate based synthesis. Although there are readily Fe_3 and/or Fe_2NiO cluster in the synthesis mixture, the lack of MOF-235 seeds as precursor results in an amorphous gel in the final product of the NO_3^- based synthesis. The possible whole transformation is illustrated in Scheme 8.1.

Anion effect: When only nitrate is used, the solid products are amorphous on all runs. However, when chlorate is introduced in the form of $FeCl_3.6H_2O$, MOF structures were obtained under certain conditions, and high selectivity of Cl^- is also observed, even in the case of mixed metal synthesis, there are both NO_3^- and Cl^-, only Cl^- is present in the final product. In our syntheses involving $FeCl_3.6H_2O$, $FeCl_4^-$ as balancing anion is found at the beginning of the syntheses then it gradually disappears. In fact, the necessity of halogen for the synthesis of trinuclear MOF has been reported in the synthesis of the trinuclear based MIL by several authors. [30-33];[46-48] The first report on the synthesis of Cr_3-MIL-101 mentioned the use of $Cr(NO_3)_3.9H_2O$ without chlorate, however, other halogen anion in the form of HF is required.[36] Later, Jhung et al. found out that when $CrCl_3$ is used, there is no need of HF to obtain MIL-101(Cr).[30, 31] Reports on the synthesis of Al_3-MIL-101

also emphasized the successful use of $AlCl_3$ and the infertile use of $Al(NO_3)_3$.[33, 37] Successful preparations of Fe_3-MIL-101 also involve the use of $FeCl_3.6H_2O$.[12, 38, 39] But from the experimental point of view, the difference in products obtained from different anions deserves a rational explanation. The role of ion type in the synthesis of MOF has been emphasized,[11] but so far, to the best of our knowledge, there is few comprehensive investigation published. Férey et al. suggested a vague mineral role of F^- and a possible template effect of Cl^-, but the detail is unknown.[11, 12, 40] The original formula of MOF-235 is $Fe_3O(bdc)_3.FeCl_4$ which requires Cl^-, thus strictly speaking, nitrate cannot give original MOF-235 structure. But the question is why a similar structure based one nitrate $Fe_3O(bdc)_3.NO_3$ was not observed, instead a gel is form. We believe that the difference lies in the template effect of the anion. Let's consider the case when $FeCl_4^-$ and NO_3^- residing in the pore structure. $FeCl_4^-$ is a tetrahedron of which four vertexes are Cl anion and the center is the Fe cation. The -1 charge of $FeCl_4^-$ is distributed evenly in the four Cl anions. The NO_3^- features a triangle structure with nitrogen in the center and three oxygens at the corners. The -1 charge of NO_3^- is distributed evenly in the three O anions, each carrying -2/3 charge. For every 3 Fe atoms in the cluster, one anion is needed to balance the charge. It would be safe to assume that the charge is distributed evenly among the Fe atoms in the framework. Hence a tetrahedral structure of $FeCl_4^-$ would be better at balancing the charge of its MOF surrounding than a flat structure of nitrate. However, to confirm this suggestion, comprehensive theoretical calculation and simulation would be necessary.

A similar role of compensating anion can be found in zeolite science, the role of counter ions is not only to balance the framework but also to initiate the ordering structure in the nucleation.[41-43] As zeolite framework is positive charged, the cations will assume the template role, organizing around themselves negative charged oligomers in an energetically favored fashion, thus forming certain favored geometry. This idea has been suggested since the early days of the zeolite science and has been consolidated and developed ever since, and become widely accepted.[41-44] In a similar fashion, the formation of MOF-235 could be started with the assembly of the positive charged metal carboxylate clusters around the negative charged $FeCl_4^-$ in a geometry that favors the formation of the **acs** net of MIL-235. The bulkier and more spacious of $FeCl_4^-$ is a template guiding the formation of ordered structure, while the nitrate is less effective resulting in

disordered structure. The possible mechanism is illustrated in Scheme 8.2. Beside the anions, the template effect can be drawn from the use of bulky and appropriate terminal ligand such as CH_3CN as reported by Choi et al.[28] Other possible ligands could be pyridine, THF. Bulkier linkers could also provide a template effect.[45] The use of functional bdc (NH_2-bdc) could improve the selection of MOF-235 as well as MIL-88B without the need of chlorate.[29] The steric hindrance of the function group could stabilize and increasing the preference of MOF-235 structure over the amorphous solid.

7.5. Conclusion

The synthesis of Fe_2Ni-MIL-88B provides us an opportunity to have a detailed investigation of the synthesis of MOF. We found in it many aspects of crystal nucleation and growth: phase transformation, phase selectivity, precursor and template. The key to the explanation of all these phenomena is to understand the kinetic and thermodynamic difference between Fe_3O and Fe_2NiO. Fe_3O is kinetically favored while Fe_2NiO is thermodynamically favored. $FeCl_4^-$ anion is suggested to be template for the formation of MOF-235 as well as the MIL-88B structure. Although our suggestions on the mechanisms and the anion effect are in agreement with the experiment results, a theoretical calculation is actually needed.

We also notice resemblances between zeolite science and MOF science. In fact, concepts and ideas that have been well developed in the synthesis of zeolite such as: template, SBU (secondary unit building), seeding, aging etc. can be used and applied to MOF synthesis. In return, it is hoped that advances in MOF science could also inspire new discovery in zeolites.

†Electronic Supplementary Information (ESI) available: Details of FTIR spectra HRTEM and EDS spectra. See DOI: 10.1039/b000000x/

References

1 H.-C. Zhou, J. R. Long, O. M. Yaghi, *Chem. Rev.* **2012**, *112*, 673.
2 H. Li, M. Eddaoudi, M. O'Keeffe, O. M. Yaghi, *Nature* **1999**, *402*, 276.
3 A. Corma, H. García, F. X. Llabrés i Xamena, *Chem. Rev.* **2010**, *110*, 4606.
4 P. Horcajada, R. Gref, T. Baati, P. K. Allan, G. Maurin, P. Couvreur, G. Férey, R. E. Morris, C. Serre, *Chem. Rev.* **2011**, *112*, 1232.
5 P. Horcajada, T. Chalati, C. Serre, B. Gillet, C. Sebrie, T. Baati, J. F. Eubank, D. Heurtaux, P. Clayette, C. Kreuz, J.-S. Chang, Y. K. Hwang, V. Marsaud, P.-N. Bories, L. Cynober, S. Gil, G. Ferey, P. Couvreur, R. Gref, *Nat Mater* **2010**, *9*, 172.
6 L. Mitchell, B. Gonzalez-Santiago, J. P. S. Mowat, M. E. Gunn, P. Williamson, N. Acerbi, M. L. Clarke, P. A. Wright, *Catal. Sci. Tech.* **2013**, *3*, 606.
7 A. Dhakshinamoorthy, M. Alvaro, H. Chevreau, P. Horcajada, T. Devic, C. Serre, H. Garcia, *Catal. Sci. Technol.* **2012**, *2*, 324.
8 P. Horcajada, F. Salles, S. Wuttke, T. Devic, D. Heurtaux, G. Maurin, A. Vimont, M. Daturi, O. David, E. Magnier, N. Stock, Y. Filinchuk, D. Popov, C. Riekel, G. Férey, C. Serre, *J. Am. Chem. Soc.* **2011**, *133*, 17839.
9 S. Surble, C. Serre, C. Mellot-Draznieks, F. Millange, G. Ferey, *Chem. Commun.* **2006**, 284.
10 G.-T. Vuong, M.-H. Pham, T.-O. Do, *Dalton Trans.* **2013**, *42*, 550.
11 G. Ferey, *Chem. Soc. Rev.* **2008**, *37*, 191.
12 S. Bauer, C. Serre, T. Devic, P. Horcajada, J. r. m. Marrot, G. r. Férey, N. Stock, *Inorg. Chem.* **2008**, *47*, 7568.
13 A. B. Blake, A. Yavari, *J. Chem. Soc., Chem. Commun.* **1982**, 1247.
14 A. B. Blake, A. Yavari, W. E. Hatfield, C. N. Sethulekshmi, *J. Chem. Soc., Dalton Trans.* **1985**, 2509.
15 Y. J. Kim, C. R. Park, *Inorg. Chem.* **2002**, *41*, 6211.
16 A. Fateeva, P. Horcajada, T. Devic, C. Serre, J. Marrot, J.-M. Grenèche, M. Morcrette, J.-M. Tarascon, G. Maurin, G. Férey, *Eur. J. Inorg. Chem.* **2010**, *2010*, 3789.
17 K. Nakamoto, *Infrared spectra of inorganic and coordination compounds*, Wiley-Interscience New York 1986.
18 R. D. Cannon, R. P. White, in *Prog. Inorg. Chem.*, Vol. 36, John Wiley & Sons, Inc., 1988, 195.
19 G. Xue, *Prog. Polym. Sci.* **1994**, *19*, 317.
20 J. F. Arenas, J. I. Marcos, *Spectrochim. Acta, Part A* **1979**, *35*, 355.
21 J. F. Arenas, J. I. Marcos, *Spectrochim. Acta, Part A* **1980**, *36*, 1075.
22 P. Larkin, *Infrared and Raman Spectroscopy; Principles and Spectral Interpretation*, Elsevier, Amsterdam 2011.
23 M. K. Johnson, D. B. Powell, R. D. Cannon, *Spectrochim. Acta, Part A* **1981**, *37*, 995.
24 H. Hellman, R. S. Laitinen, L. Kaila, J. Jalonen, V. Hietapelto, J. Jokela, A. Sarpola, J. Rämö, *J. Mass Spectrom.* **2006**, *41*, 1421.
25 M. S. Sitze, E. R. Schreiter, E. V. Patterson, R. G. Freeman, *Inorg. Chem.* **2001**, *40*, 2298.
26 J. Sanders-Loehr, W. D. Wheeler, A. K. Shiemke, B. A. Averill, T. M. Loehr, *J. Am. Chem. Soc.* **1989**, *111*, 8084.
27 A. Ianoul, T. Coleman, S. A. Asher, *Anal. Chem.* **2002**, *74*, 1458.
28 W. Cho, S. Park, M. Oh, *Chem. Commun.* **2011**, *47*, 4138.

29 M.-H. Pham, G.-T. Vuong, A.-T. Vu, T.-O. Do, *Langmuir* **2011**, *27*, 15261.
30 N. A. Khan, S. H. Jhung, *Cryst. Growth Des* **2010**, *10*, 1860.
31 N. A. Khan, J. W. Jun, S. H. Jhung, *Eur. J. Inorg. Chem.* **2010**, *2010*, 1043.
32 F. Millange, M. I. Medina, N. Guillou, G. Férey, K. M. Golden, R. I. Walton, *Angew. Chem. Int. Ed.* **2010**, *49*, 763.
33 E. Stavitski, M. Goesten, J. Juan-Alcañiz, A. Martinez-Joaristi, P. Serra-Crespo, A. V. Petukhov, J. Gascon, F. Kapteijn, *Angew. Chem. Int. Ed.* **2011**, *50*, 9624.
34 N. W. Ockwig, O. Delgado-Friedrichs, M. O'Keeffe, O. M. Yaghi, *Acc. Chem. Res.* **2005**, *38*, 176.
35 C. Serre, C. Mellot-Draznieks, S. Surble, N. Audebrand, Y. Filinchuk, G. Ferey, *Science* **2007**, *315*, 1828.
36 G. Férey, C. Mellot-Draznieks, C. Serre, F. Millange, J. Dutour, S. Surblé, I. Margiolaki, *Science* **2005**, *309*, 2040.
37 P. Serra-Crespo, E. V. Ramos-Fernandez, J. Gascon, F. Kapteijn, *Chem. Mater.* **2011**, *23*, 2565.
38 P. F. G. S. C. G. R. C. P. Horcajada-cortes, *US Patent 20100226991*, 2010.
39 K. M. L. Taylor-Pashow, J. D. Rocca, Z. Xie, S. Tran, W. Lin, *J. Am. Chem. Soc.* **2009**, *131*, 14261.
40 D.-Y. Hong, Y. K. Hwang, C. Serre, G. Férey, J.-S. Chang, *Adv. Funct. Mater.* **2009**, *19*, 1537.
41 D. W. Breck, *Zeolite molecular sieves: structure, chemistry, and use*, Wiley, London 1973.
42 C. S. Cundy, P. A. Cox, *Chem. Rev.* **2003**, *103*, 663.
43 C. S. Cundy, P. A. Cox, *Microporous Mesoporous Mater.* **2005**, *82*, 1.
44 G.-T. Vuong, T.-O. Do, *J. Am. Chem. Soc.* **2007**, *129*, 3810.
45 P. Horcajada, F. Salles, S. Wuttke, T. Devic, D. Heurtaux, G. Maurin, A. Vimont, M. Daturi, O. David, E. Magnier, N. Stock, Y. Filinchuk, D. Popov, C. Riekel, G. Férey, C. Serre, *J. Am. Chem. Soc.* **2011**, *133*, 17839.
46 L. Meesuk, U. A. Jayasooriya, R. D. Cannon, *Spectrochim. Acta, Part A* **1987**, *43*, 687.
47 R. Wu, U. A. Jayasooriya, R. D. Cannon, *Spectrochim. Acta, Part A* **2000**, *56*, 575.
48 L. Montri, R. D. Cannon, *Spectrochim. Acta, Part A* **1985**, *41*, 643.
49 A. C. Sudik, A. P. Côté, O. M. Yaghi, *Inorg. Chem.* **2005**, *44*, 2998.

FIGURE CAPTIONS, SCHEMES AND TABLES

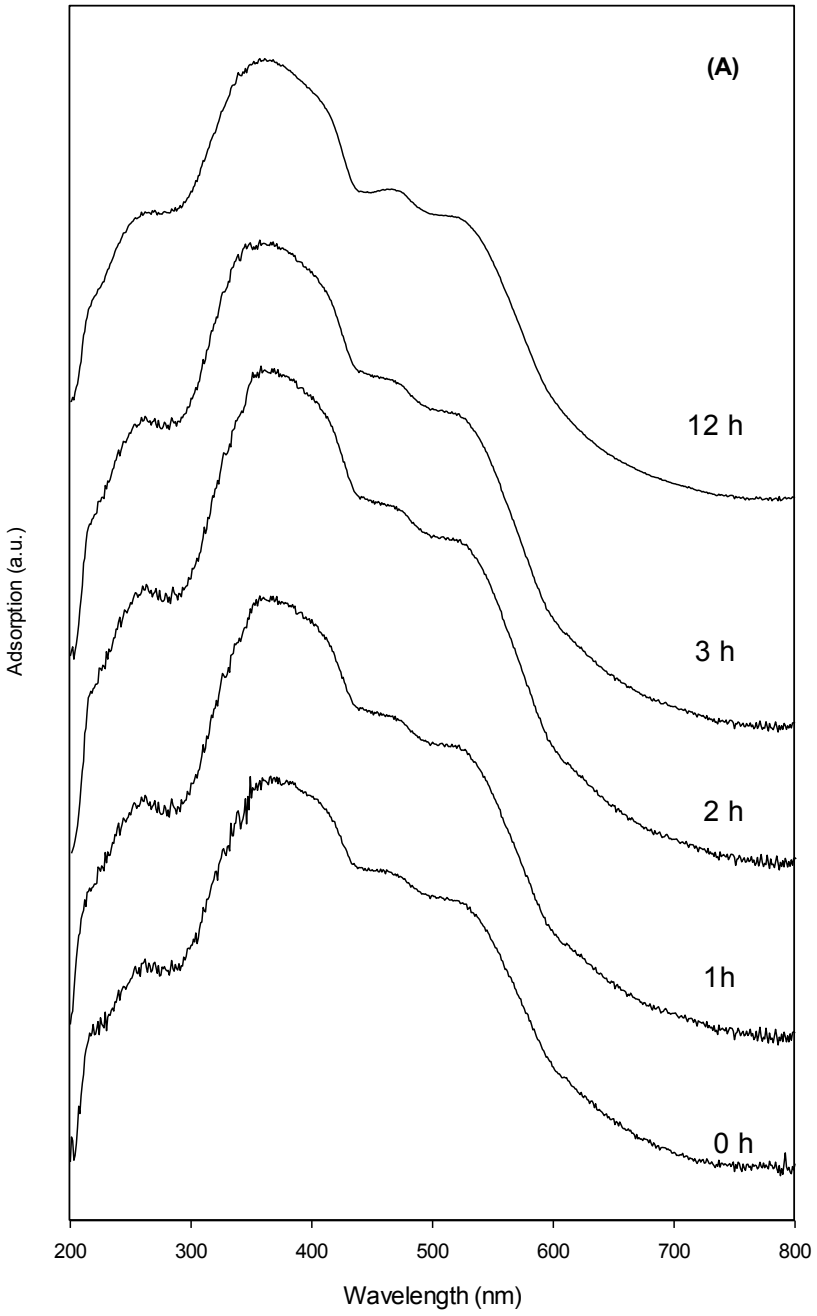

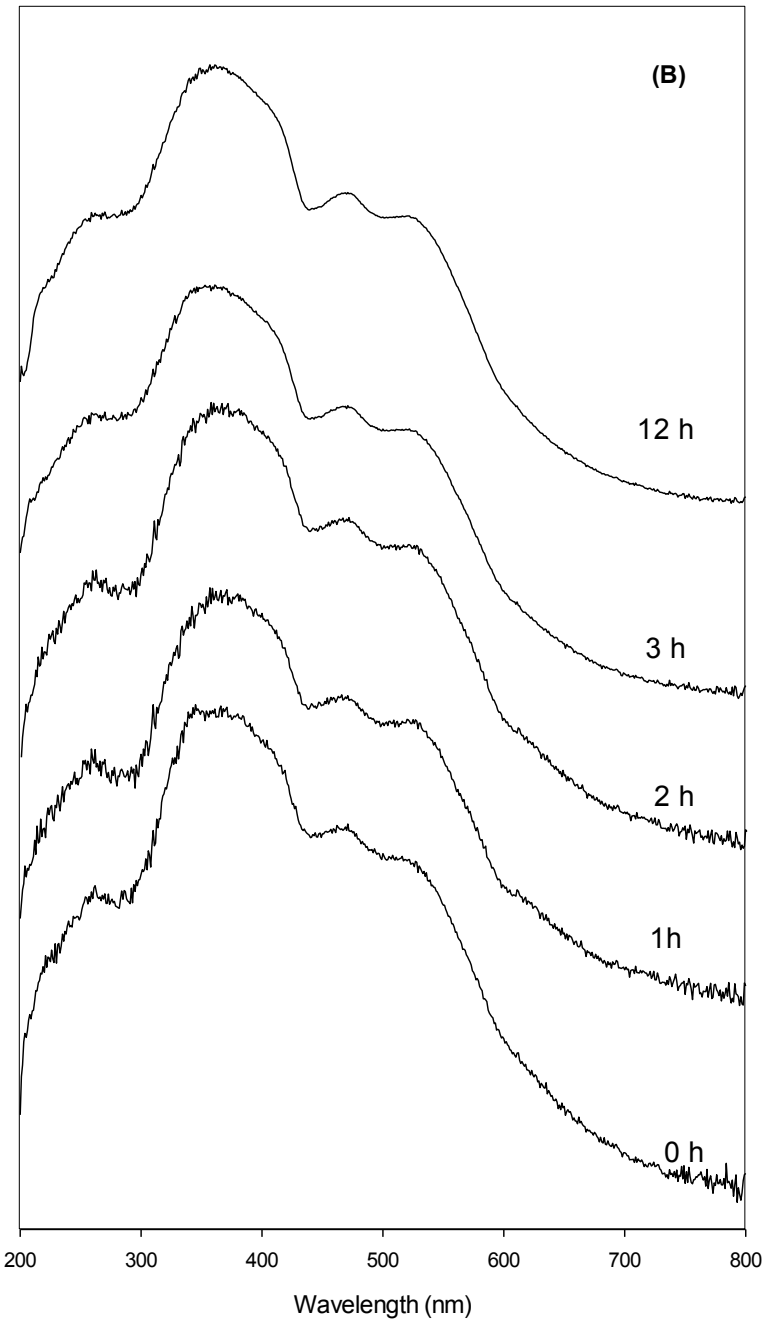

Figure 7.1. UV-Vis spectra of the samples Fe_3-NO_3-x (A) and Fe_3-Cl-x (B) prepared using $Fe(NO_3)_3.9H_2O$ and $FeCl_3.6H_2O$, respectively, at different synthesis times.

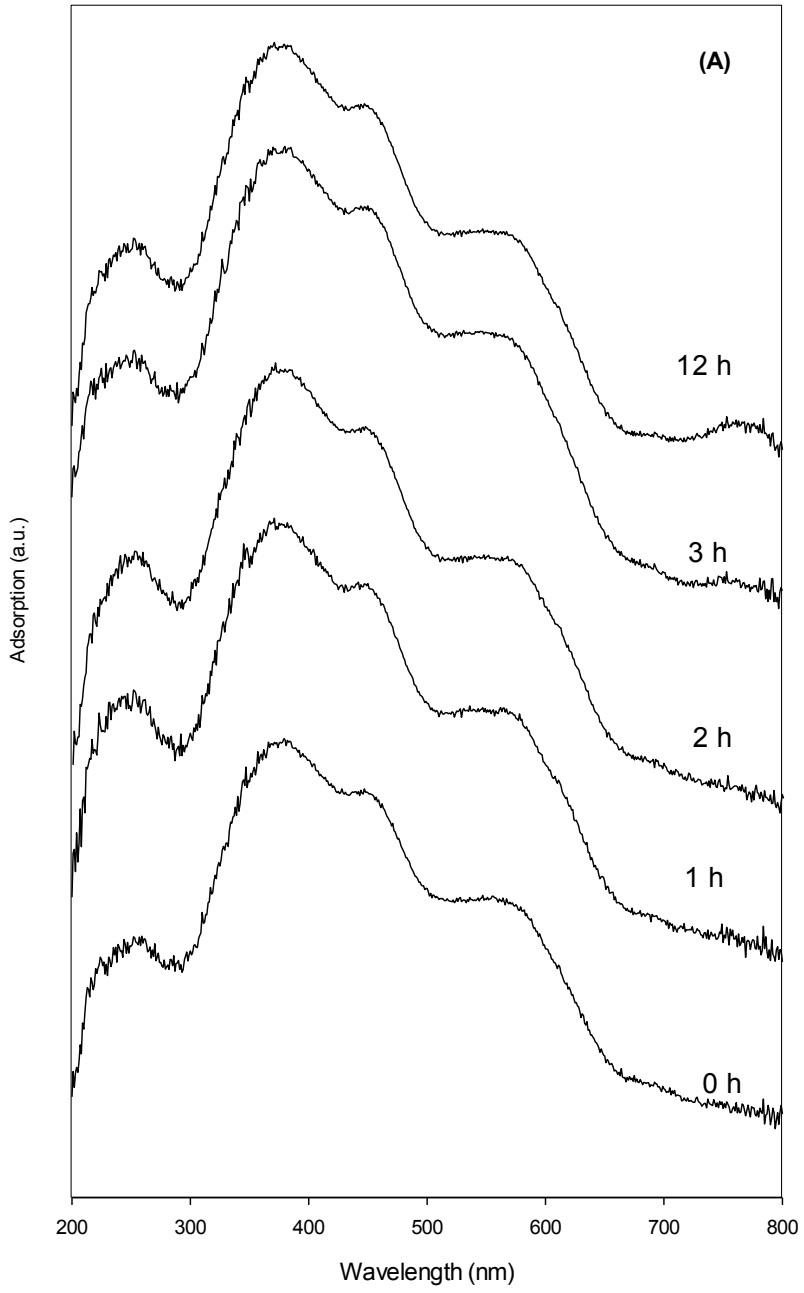
(A)
12 h
3 h
2 h
1 h
0 h
Adsorption (a.u.)
200
300
400
500
600
700
800
Wavelength (nm)

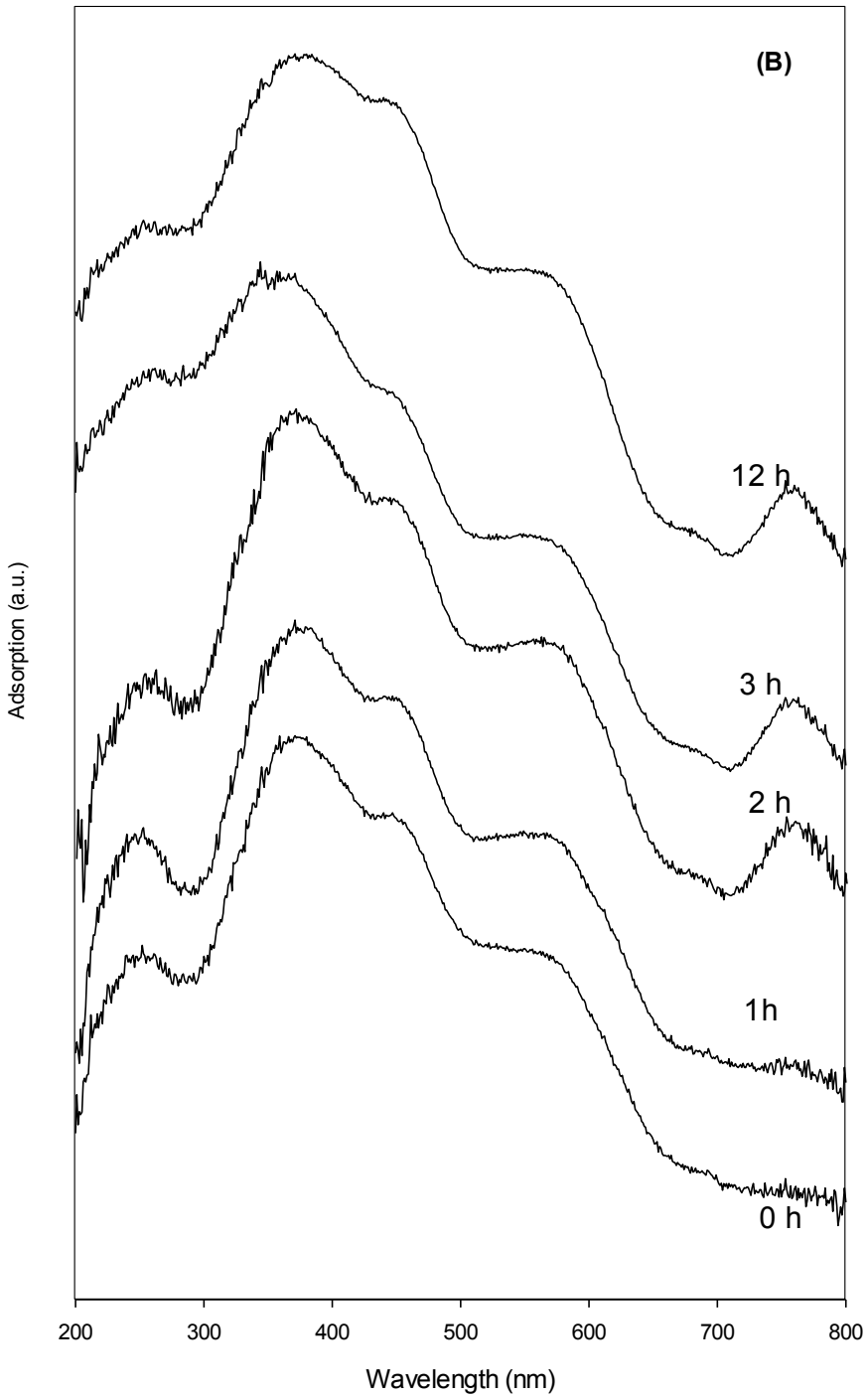

Figure 7.2. UV-Vis spectra of Fe_2Ni-NO_3-x (A) and Fe_2Ni-Cl-x (B) samples prepared using $Fe(NO_3)_3.9H_2O$ and $FeCl_3.6H_2O$, respectively at different synthesis times

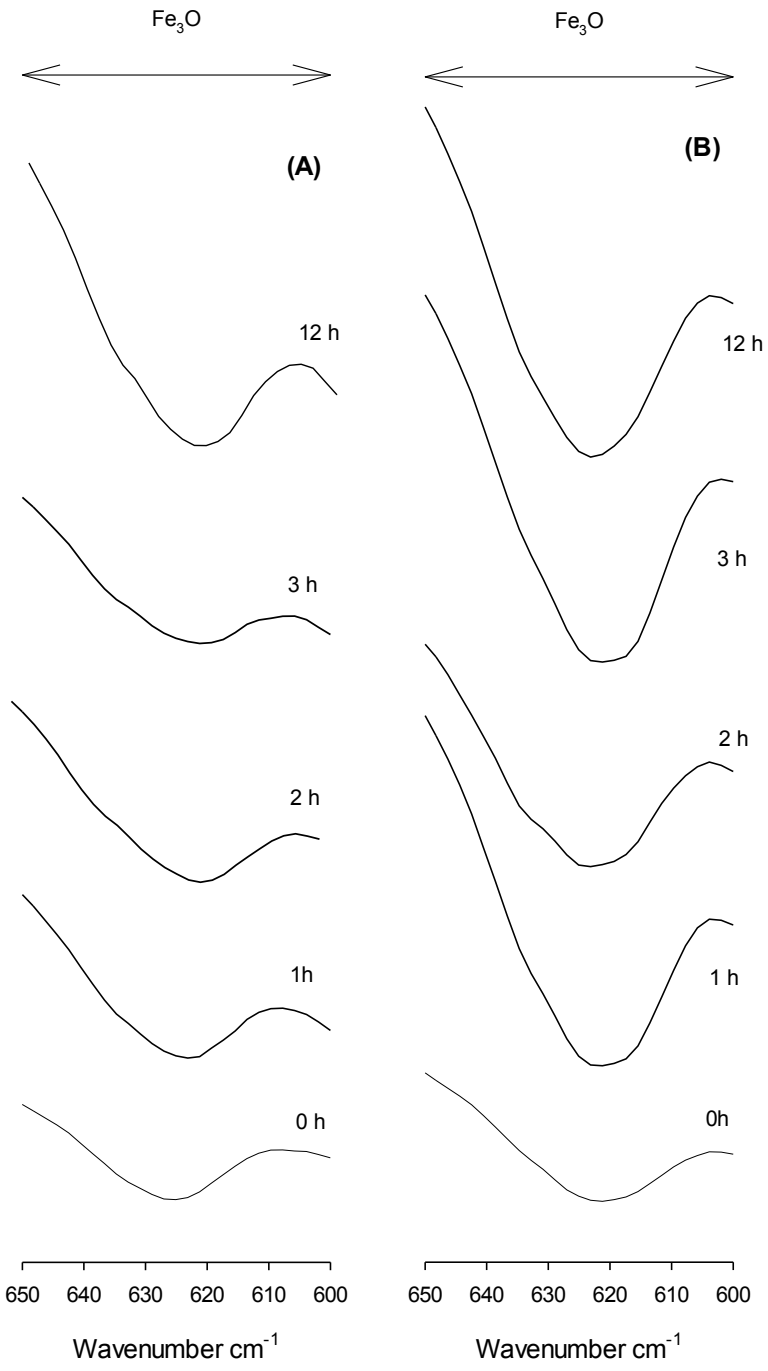

Figure 7.3. Transmittance FTIR spectra of the samples of Fe_3-NO_3-x (A) and Fe_3-Cl-x (B) at different synthesis times

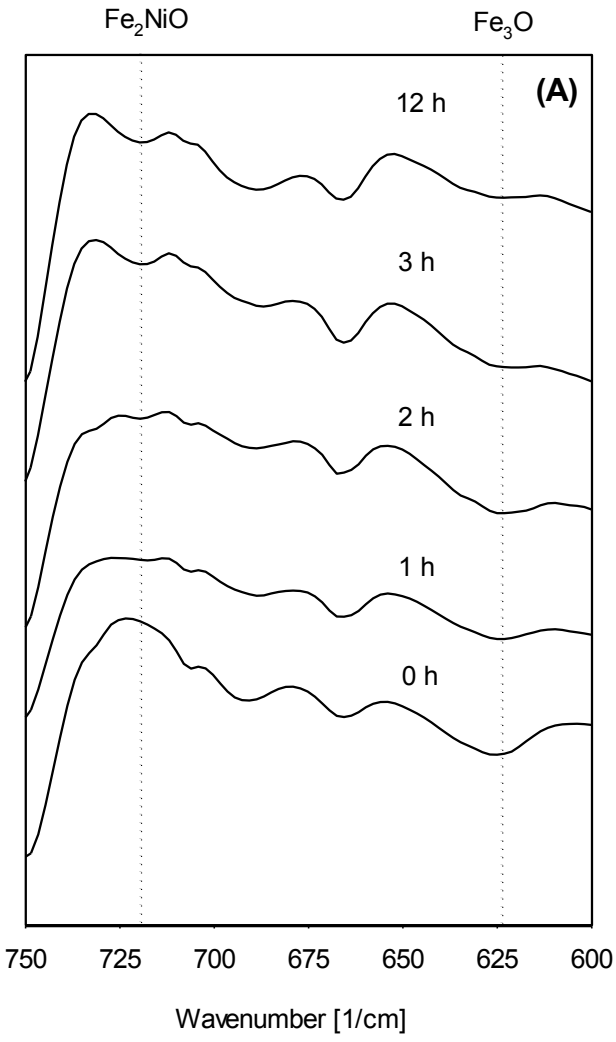
Fe2NiO
Fe3O
(A)
12 h
3 h
2 h
1 h
0 h
750
725
700
675
650
625
600
Wavenumber [1/cm]

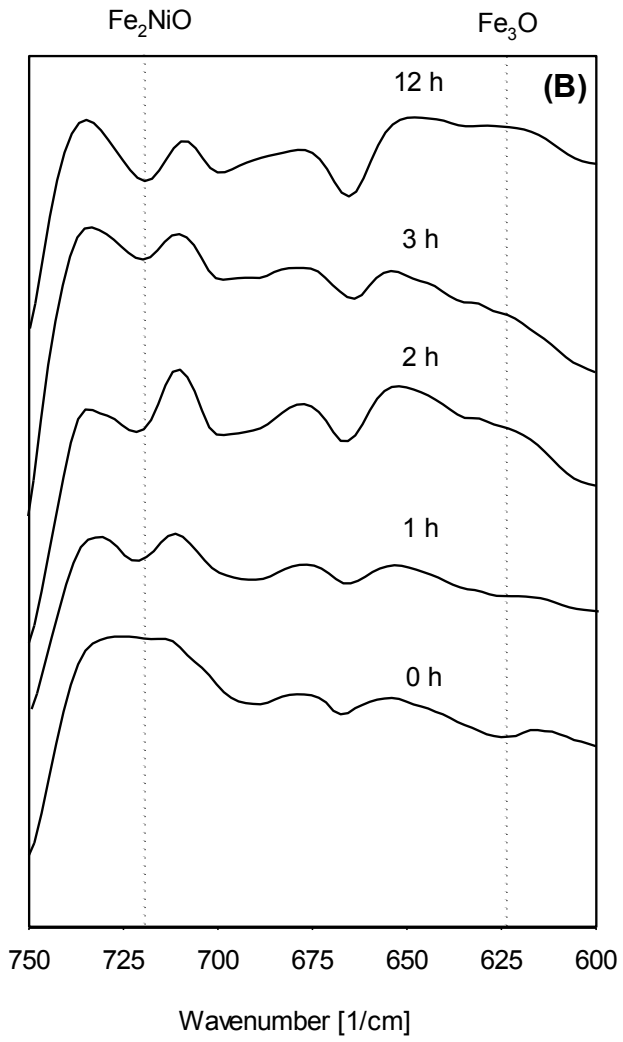

Figure 7.4. Transmittance FTIR spectra of Fe_2Ni-NO_3-x (A) and Fe_2Ni-Cl-x (B) at different synthesis times

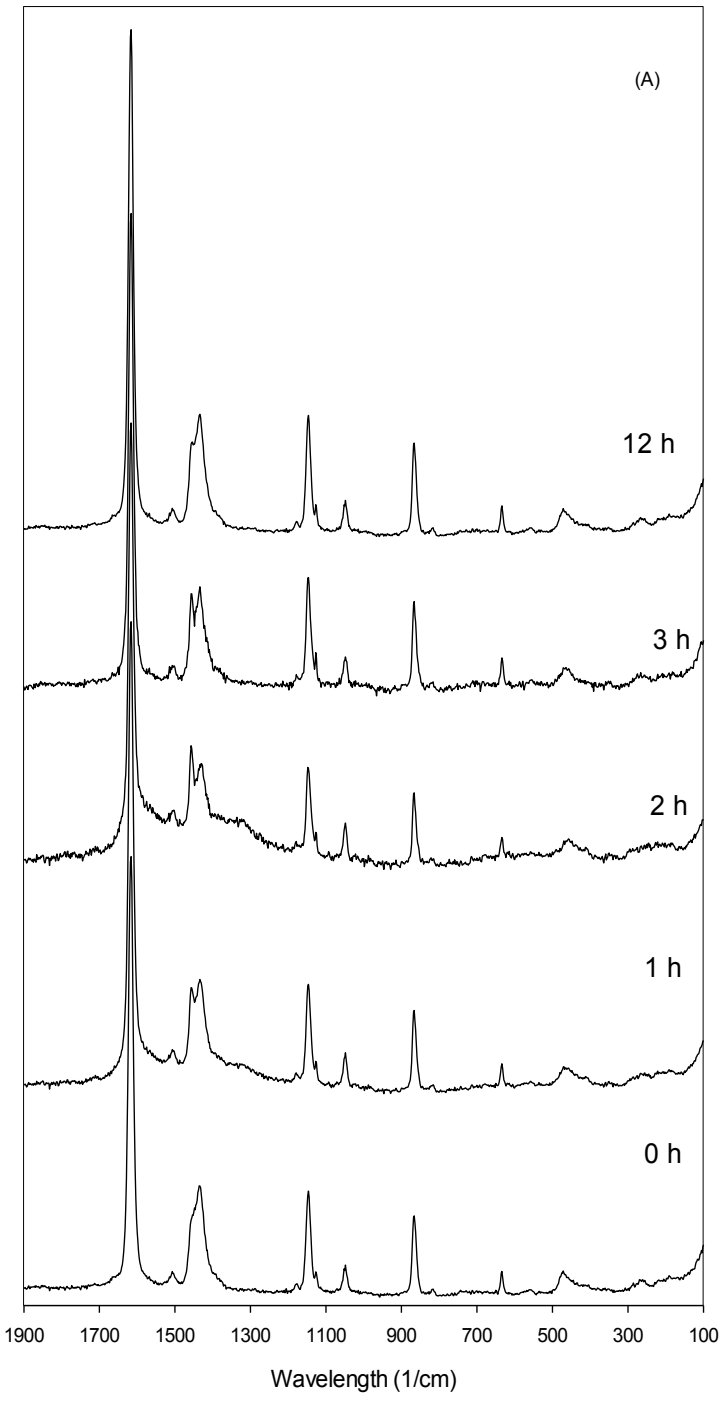
(A)
12 h
3 h
2 h
1 h
0 h
1900
1700
1500
1300
1100
900
700
500
300
100
Wavelength (1/cm)

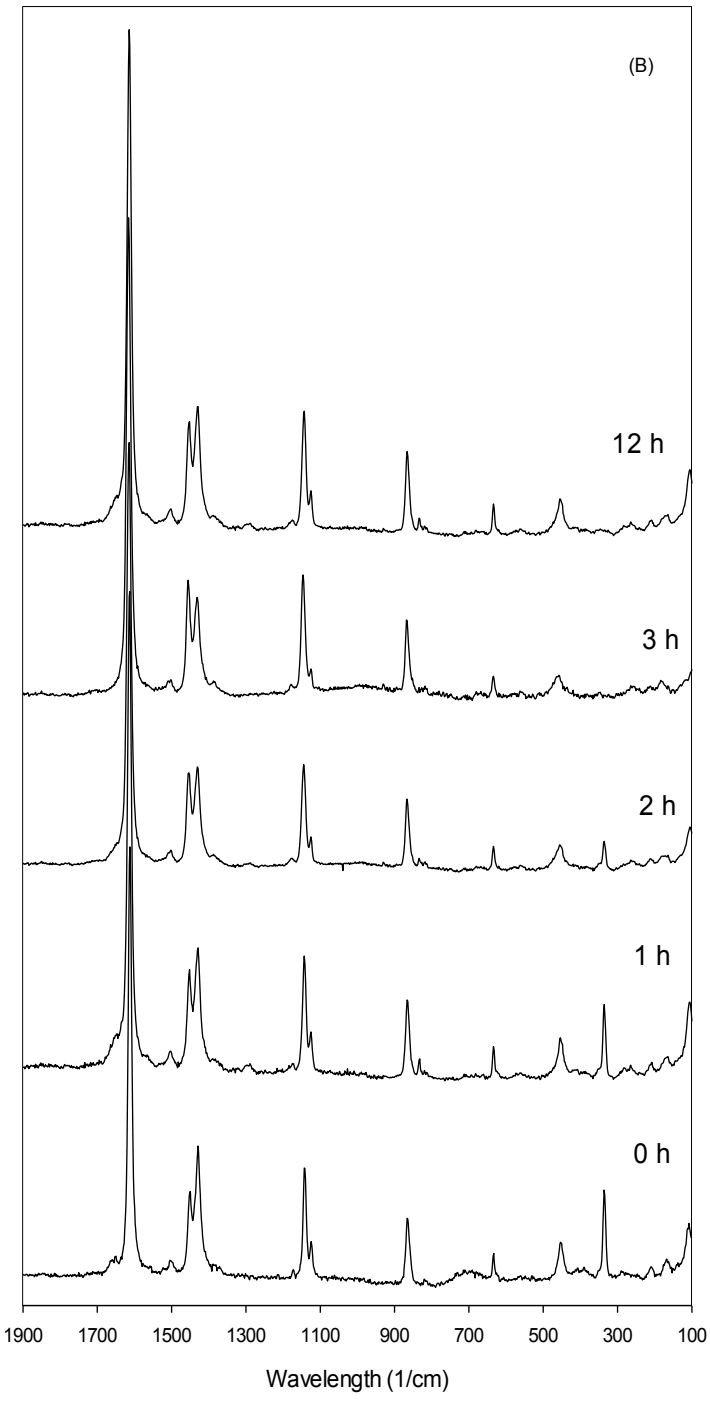

Figure 7.5. Raman spectra of the samples Fe_3-NO_3-x (A) and Fe_3-Cl-x (B) at different synthesis times

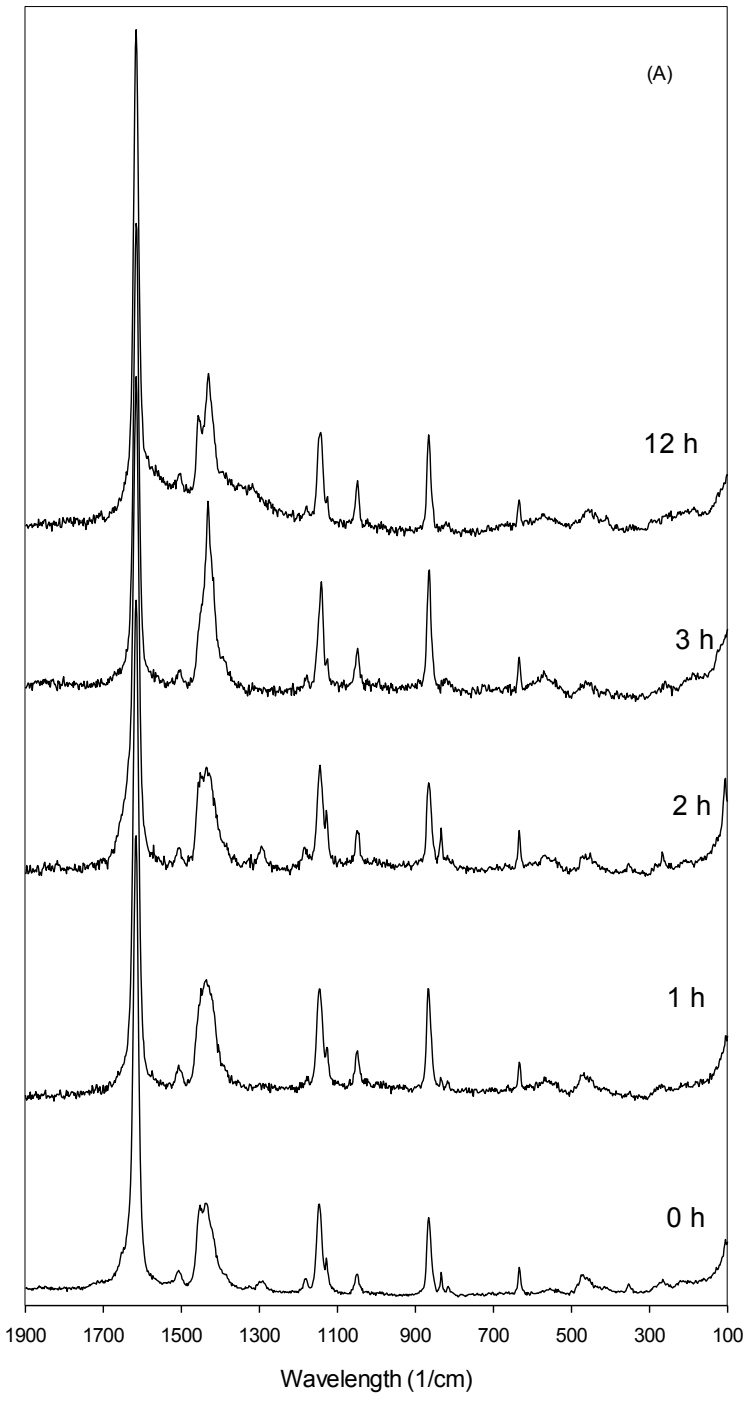
(A)
12 h
3 h
2 h
1 h
0 h
1900
1700
1500
1300
1100
900
700
500
300
100
Wavelength (1/cm)

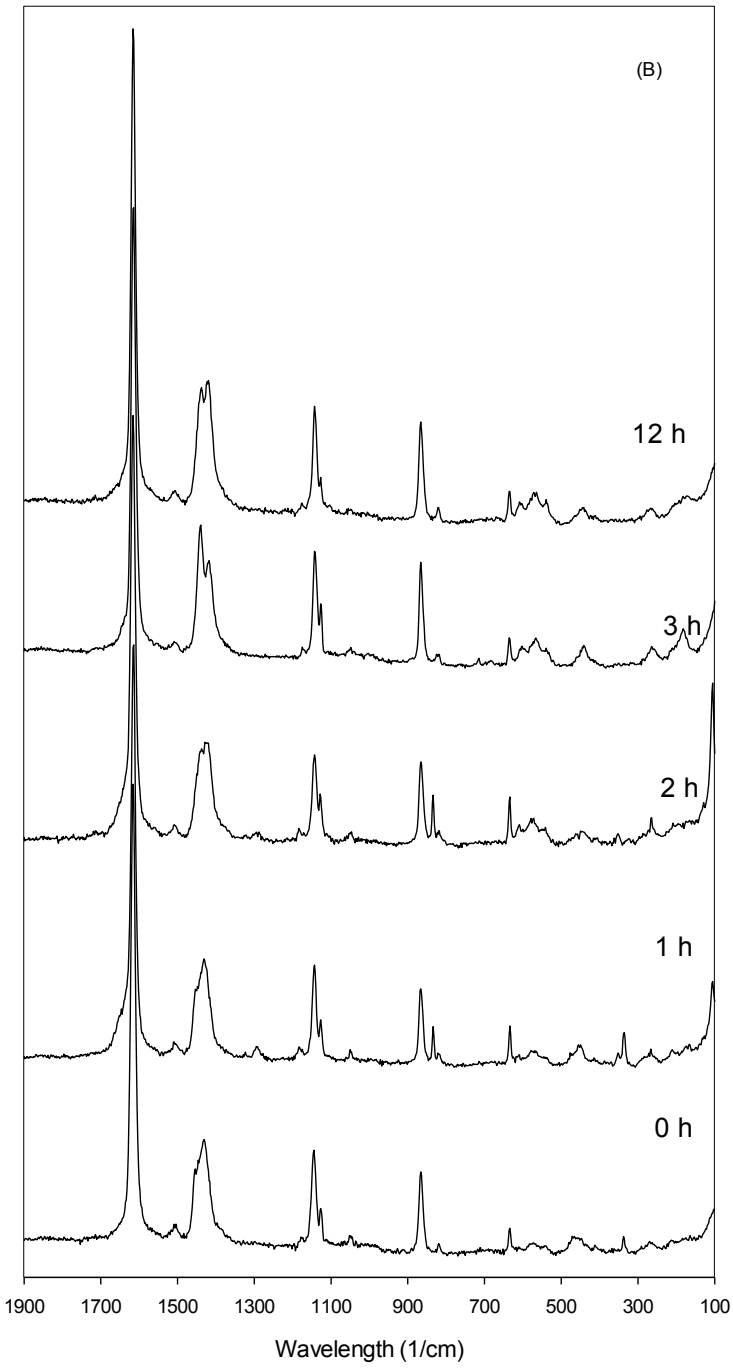

Figure 7.6. Raman spectra of Fe_2Ni-NO_3-x (A) and Fe_2Ni-Cl-x (B) at different synthesis times.

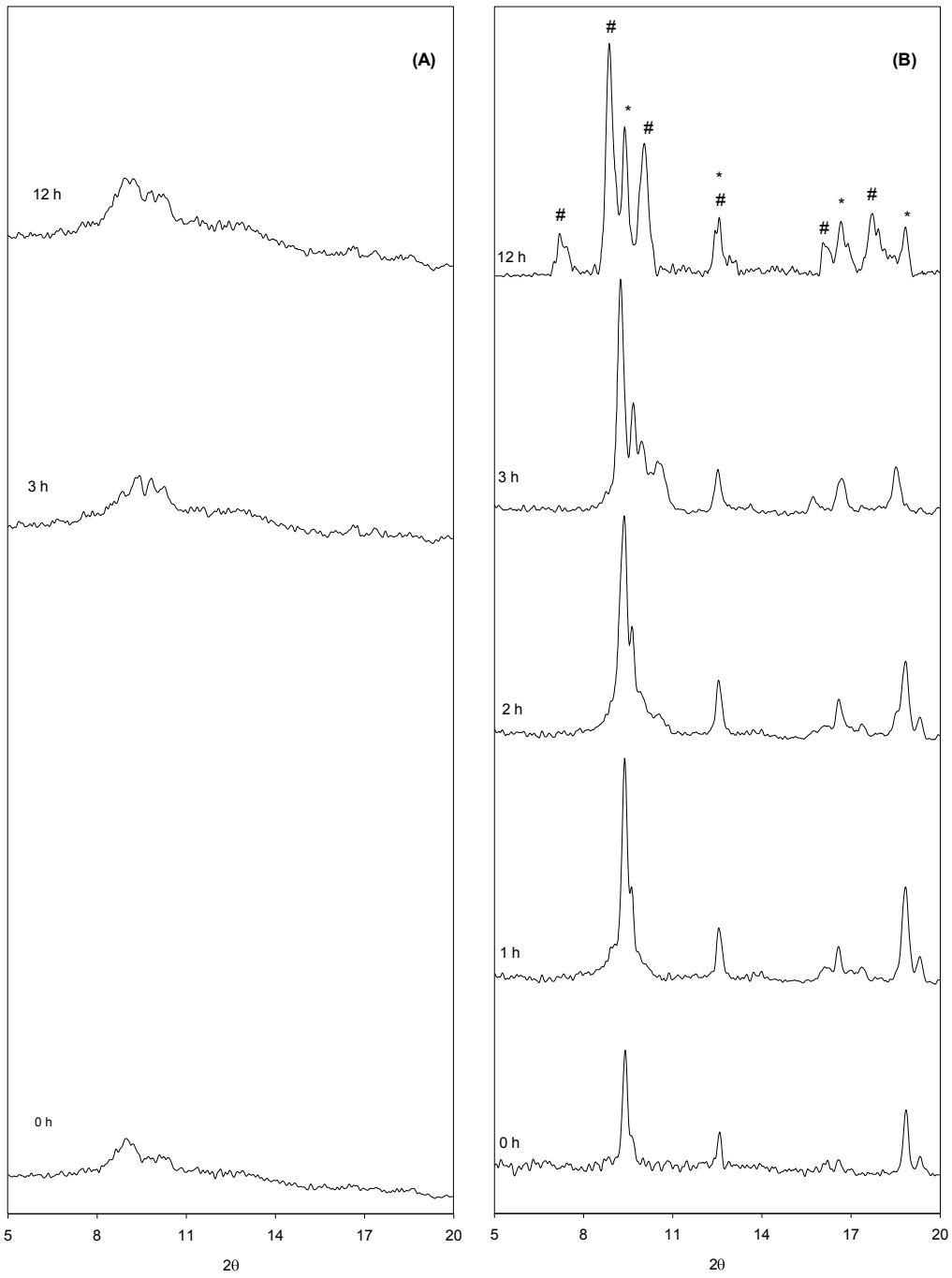

Figure 7.7. XRD patterns of Fe_3-NO_3-x (A) and Fe_3-Cl-x (B) at different synthesis times. (*) MOF-235 phase, (#): MIL-88B phase.

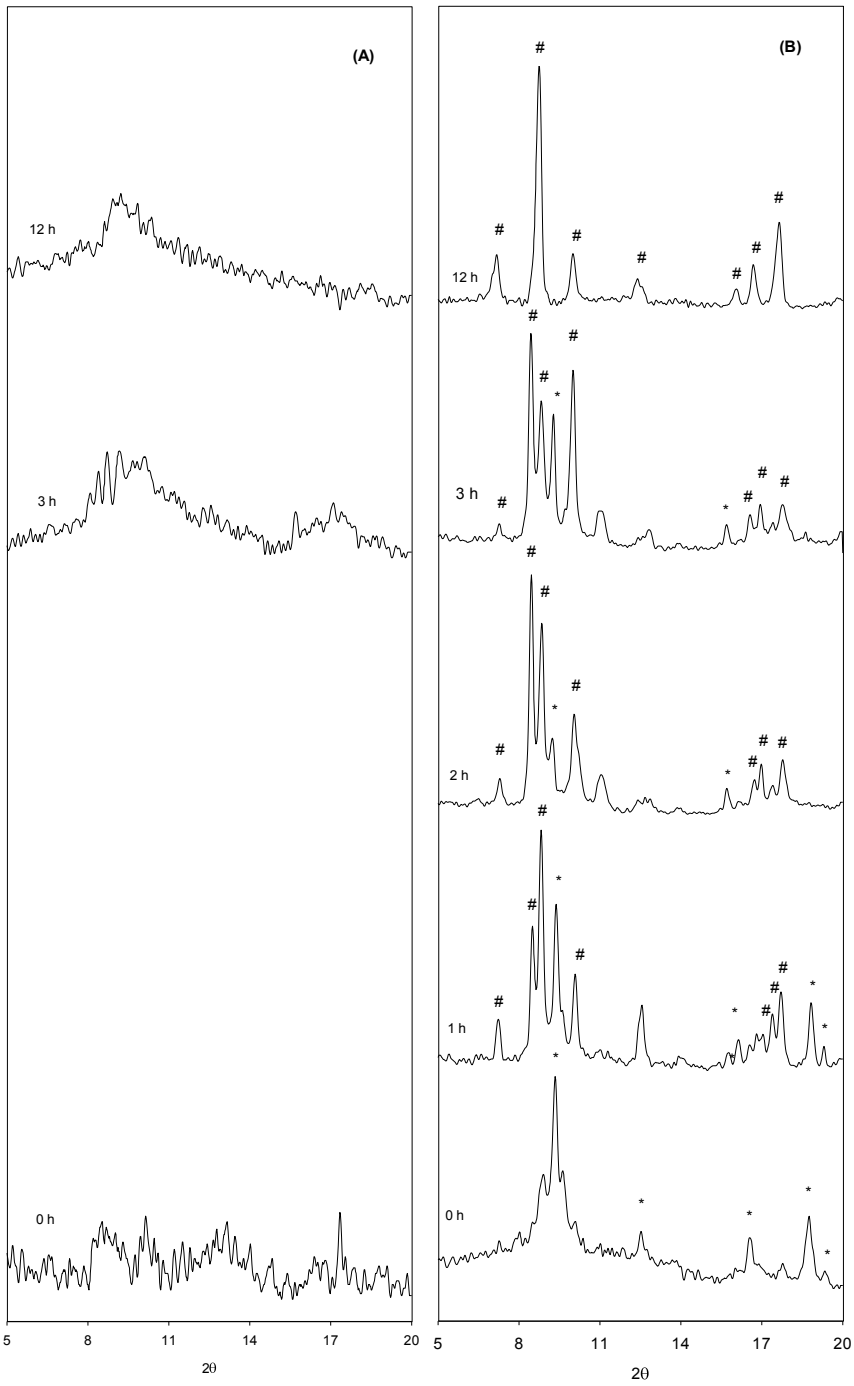

Figure 7.8. XRD patterns of Fe_2Ni-NO_3 (A) and Fe_2Ni-Cl (B) at different synthesis time. (*) MOF-235 phase, (#): MIL-88B phase

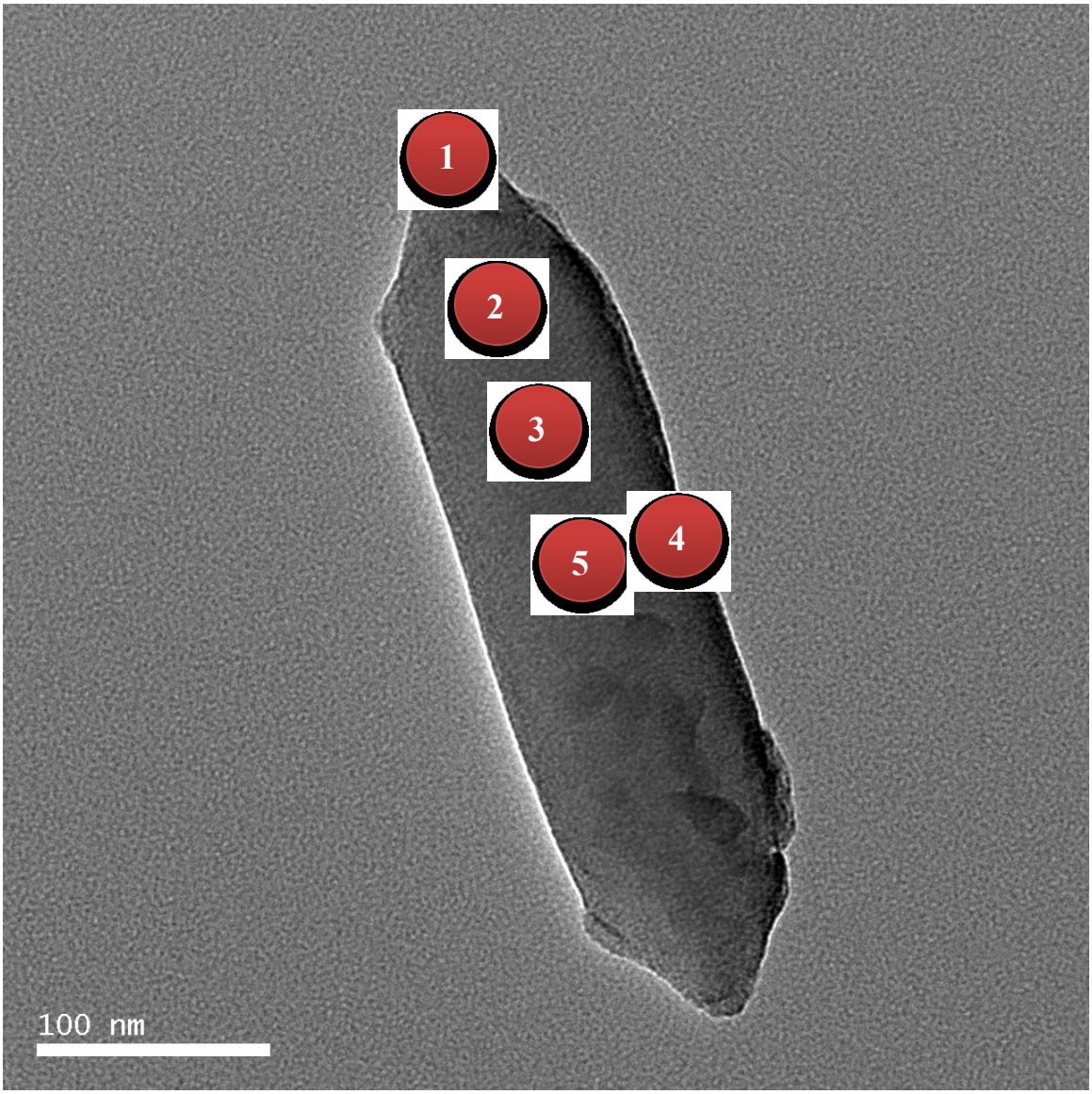

Figure 7.9. Representative HRTEM and EDS acquiring positions of Fe_2Ni-Cl-12h crystal

SCHEMES

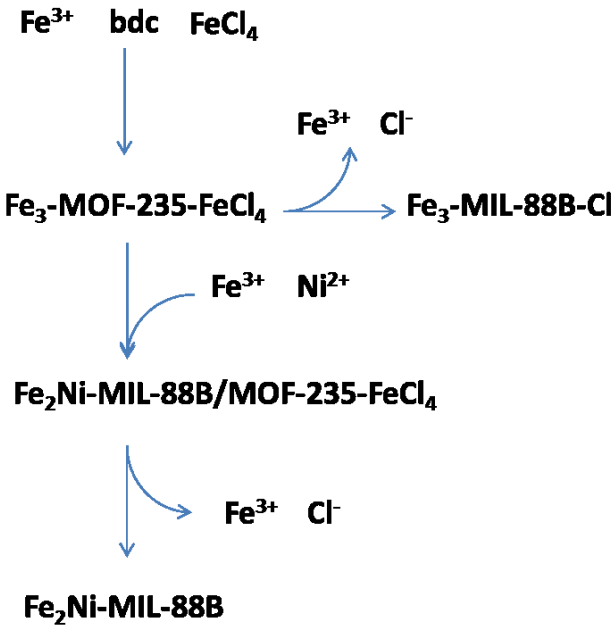

Scheme 8.1. Possible mechanism of the formation of MIL-88B samples using $FeCl_3.6H_2O$

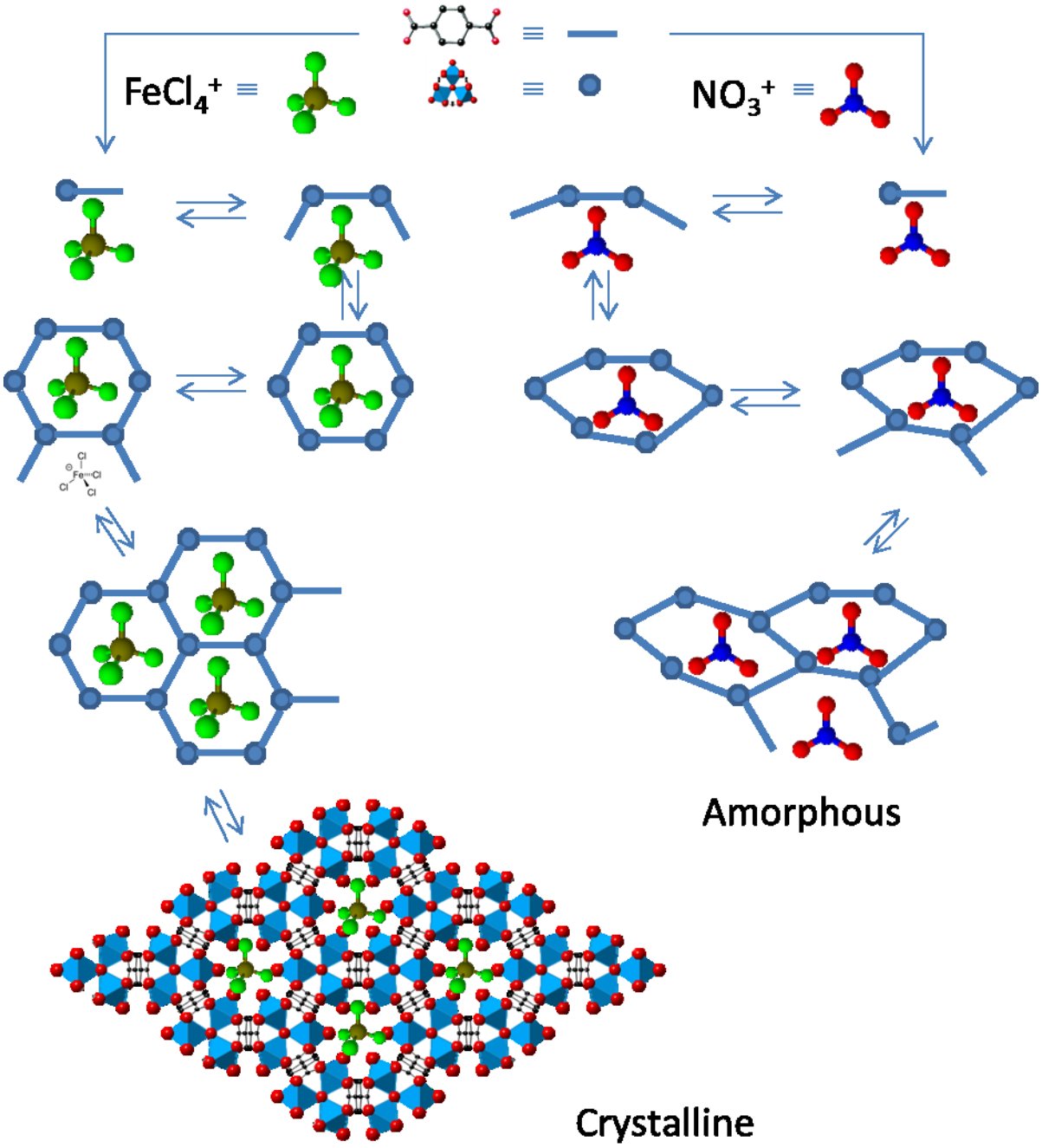

Schem 8.2. Possible proposition of anion mediated formation of MIL-88B

Table 7.1. FTIR band assignment in the wavenumber 400 – 800 cm^{-1}

Band (cm^{-1})	Assignment
750	C-H [20, 21]
720	Fe_2NiO [46, 47]
690	C-C [20, 21]
660	OCO [20, 21]
624	Fe_3O [23, 48]
550	Fe-O, Ni-O [17]

Table 7.2. Raman band assignments

Band (cm^{-1})	Assignment
175	$n_{sym}(M_3O)$
267	$\delta_{asym}(M_3O)$
330	$FeCl_4^-$
440	M-O
567	Fe_2NiO
631	OCO
860	CC
1050	NO_3-
1125	CX
1146	CH
1431	CH_3 (bending mode in DMF)
1454	CH_3 (bending mode in DMF)
1616	CC

Table 7.3. Fe and Ni atomic percentages calculated from EDS spectra

Position	Fe (atomic %)	Ni (atomic %)	Fe/Ni
1	75	36	2.1
2	67	35	2.2
3	81	29	2.8
4	78	37	2.1
5	89	19	4.7

Table 7.4. Comparison of the crystal parameters of MIL-88B and MOF-235

Parameter	MIL-88B *[9, 12]*	MOF-235 *[49]*
Chemical formula	$Fe_3O(bdc)_3Cl.3DMF$	$Fe_3O(bdc)_3FeCl_4.3DMF$
Molar weight ($g.mol^{-1}$)	905.8	1092.8
Net	acs	acs
Crystal system	Hexagonal	Hexagonal
Space group	P -6 2 c	P -6 2 c
a (Å)	11.1075	12.531
b (Å)	11.1075	12.531
c (Å)	19.0925	18.476
α	90	90
β	90	90
γ	120	120
Volume ($Å^3$)	2040.8	2512.6

Supporting Information

1. FTIR spectra of samples with wavelength 400 – 4000 cm^{-1}

1.1.Single metal synthesis using $Fe(NO_3)_3.9H_2O$

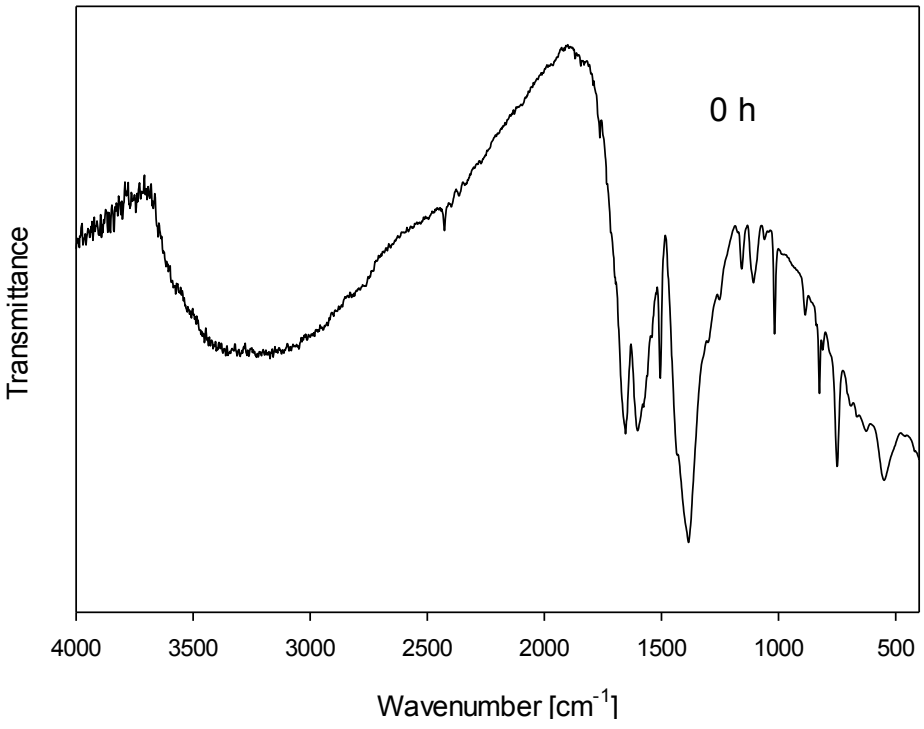

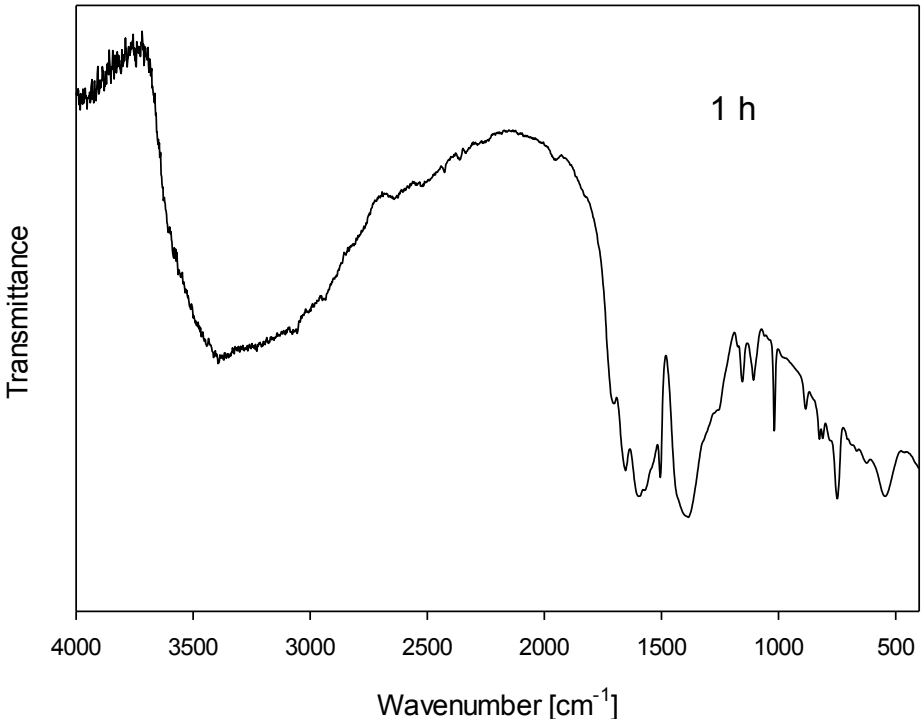

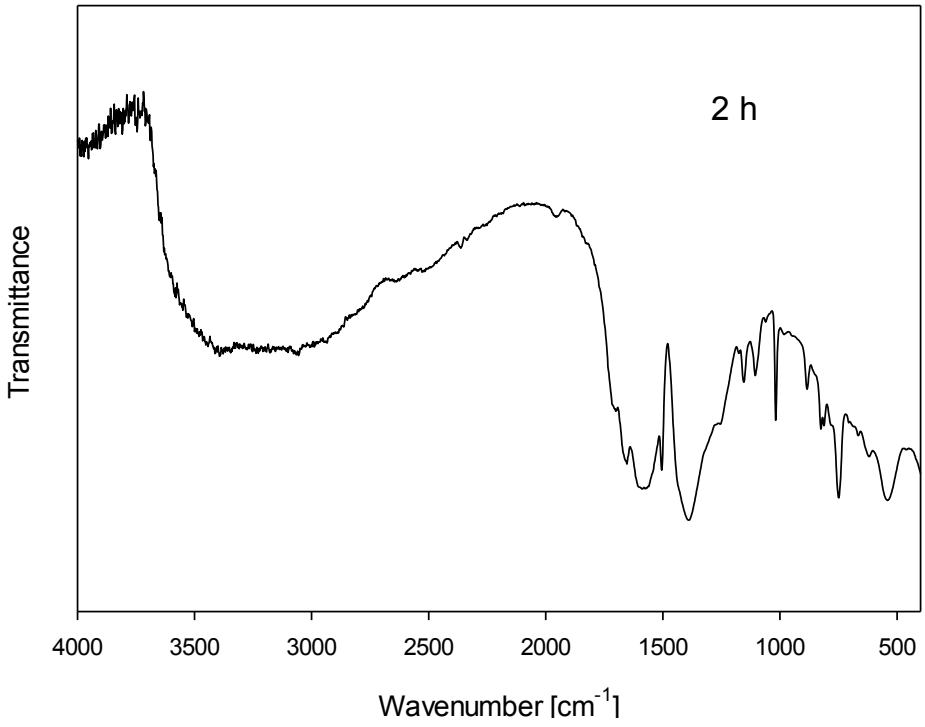
2 h
Transmittance
4000
3500
3000
2500
2000
1500
1000
500
Wavenumber [cm-1]

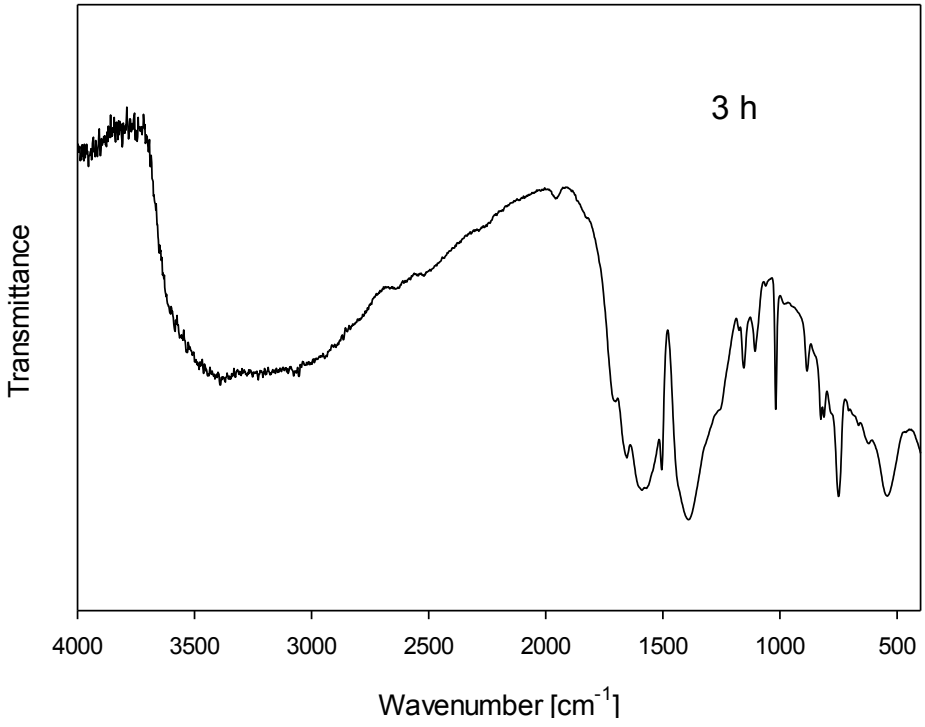
3 h
Transmittance
4000
3500
3000
2500
2000
1500
1000
500
Wavenumber [cm-1]

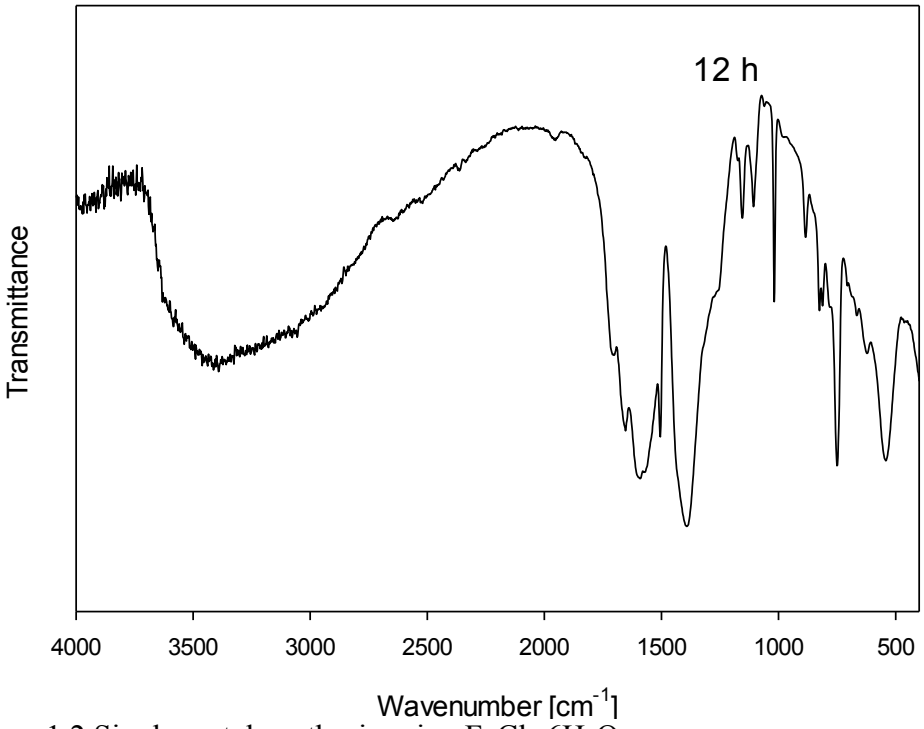

1.2.Single metal synthesis using $FeCl_3.6H_2O$

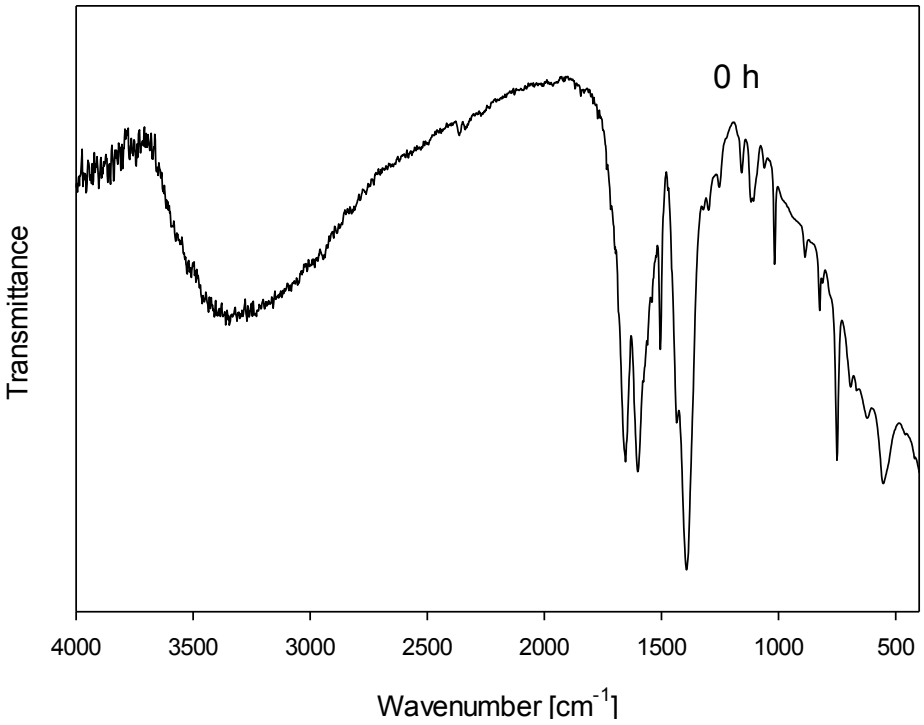

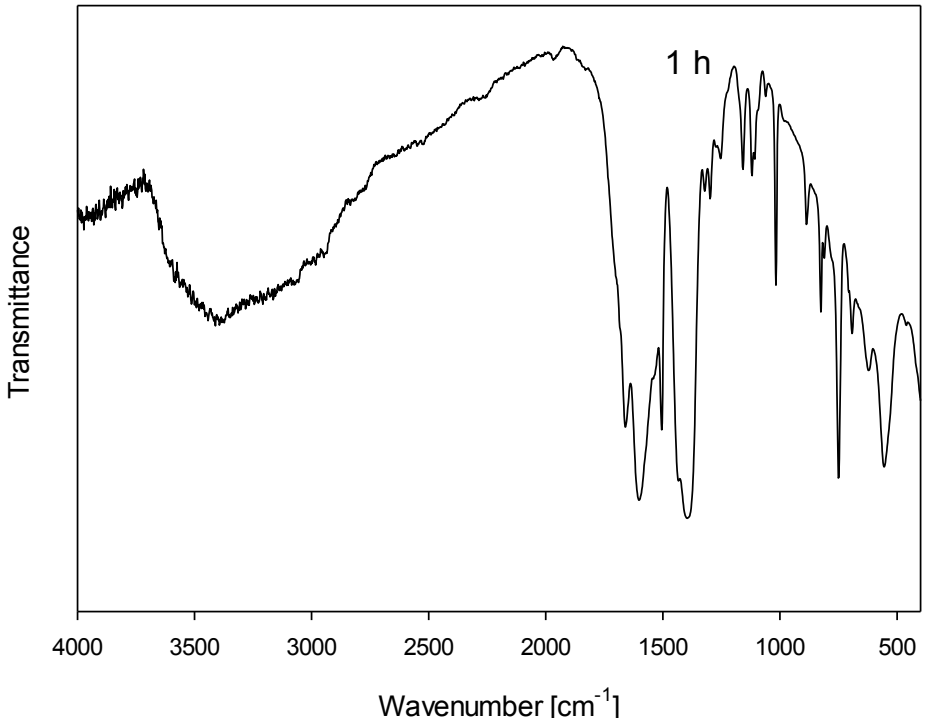
1 h
Transmittance
4000
3500
3000
2500
2000
1500
1000
500
Wavenumber [cm-1]

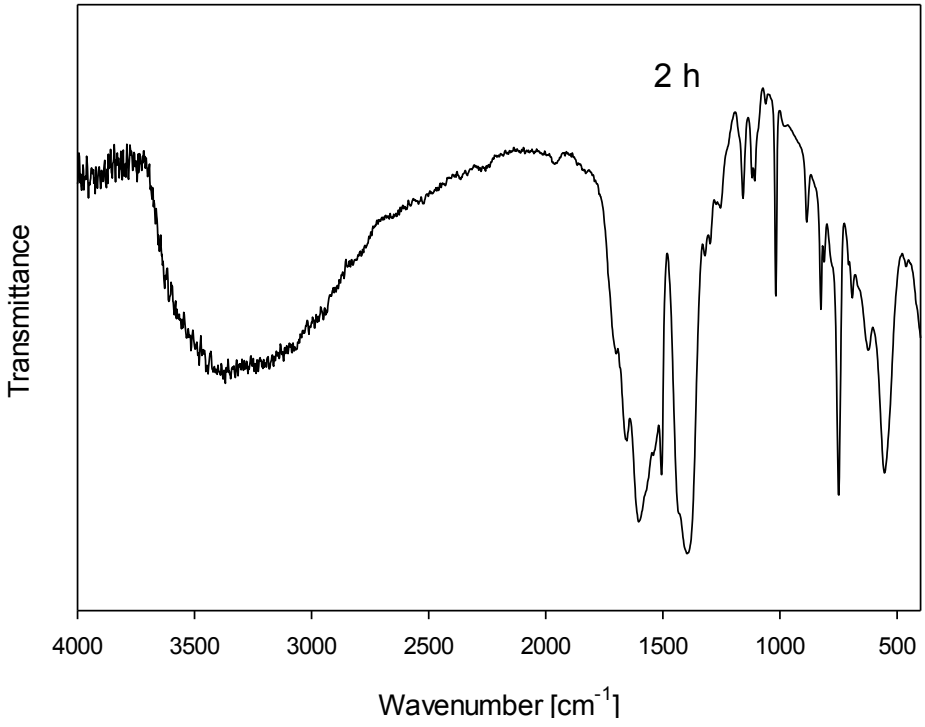
2 h
Transmittance
4000
3500
3000
2500
2000
1500
1000
500
Wavenumber [cm-1]

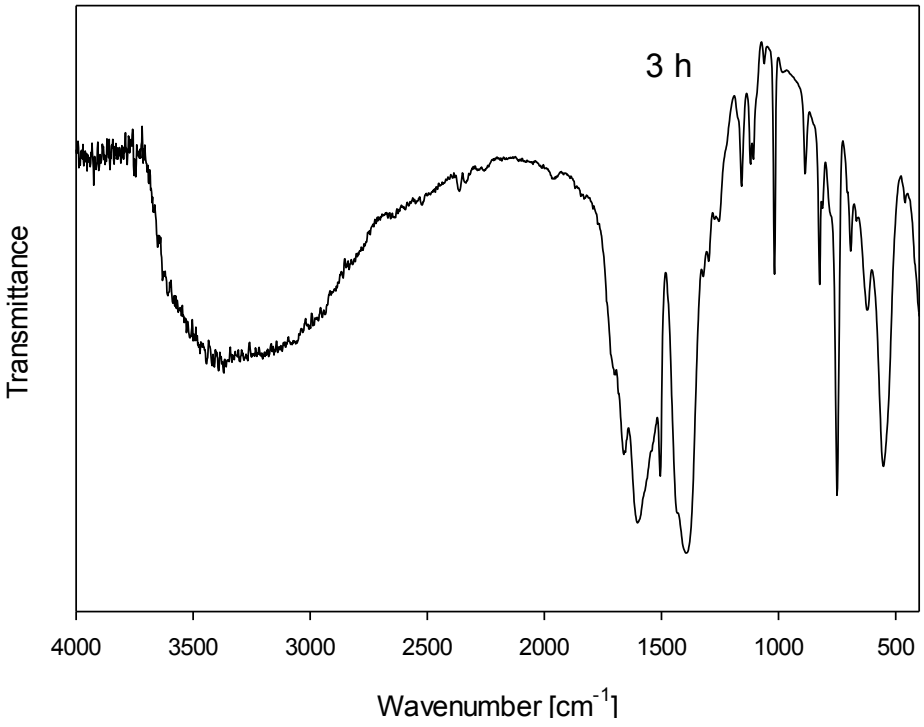

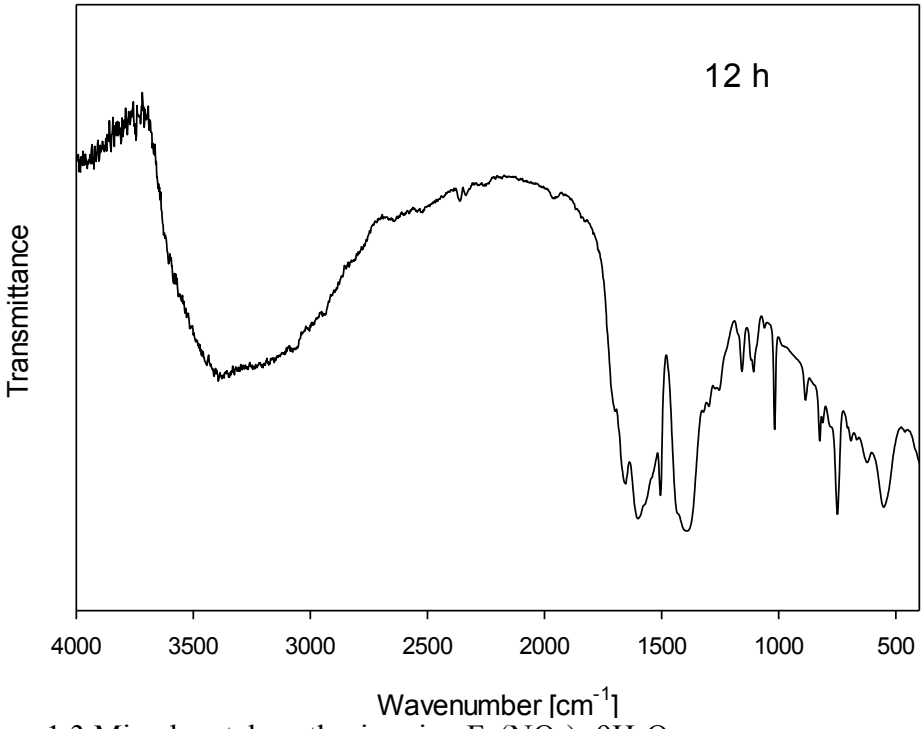

1.3.Mixed metal synthesis using $Fe(NO_3)_3.9H_2O$

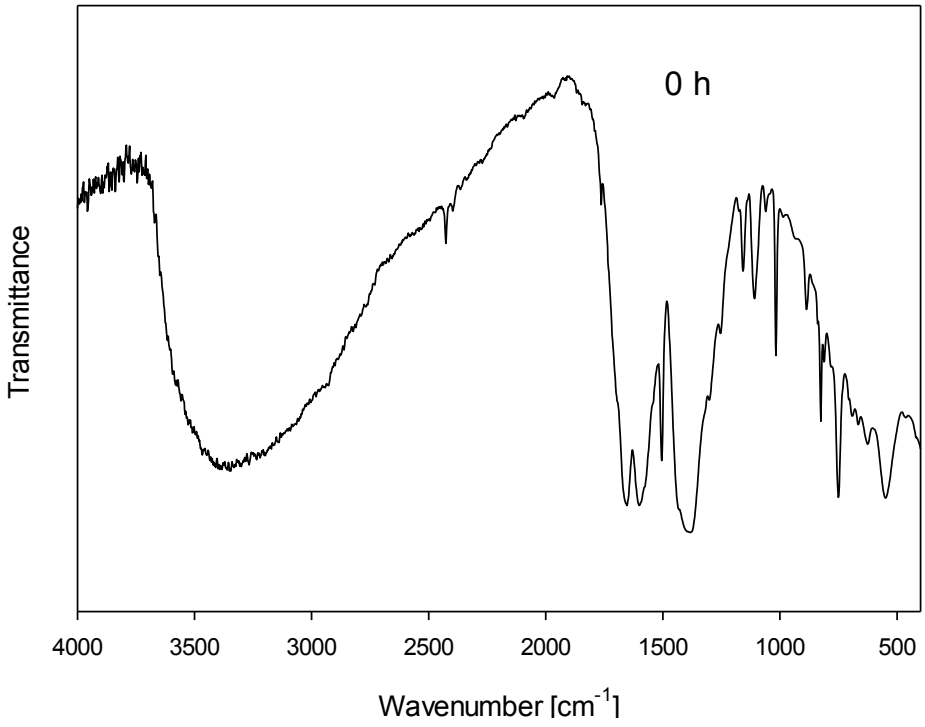
0 h
Transmittance
4000
3500
3000
2500
2000
1500
1000
500
Wavenumber [cm-1]

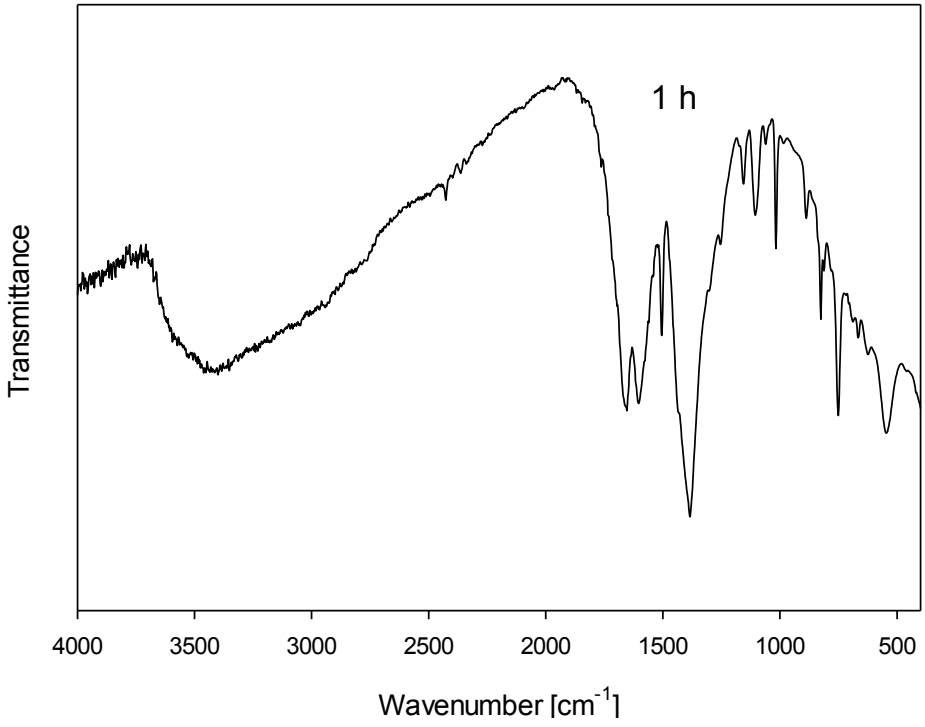
1 h
Transmittance
4000
3500
3000
2500
2000
1500
1000
500
Wavenumber [cm-1]

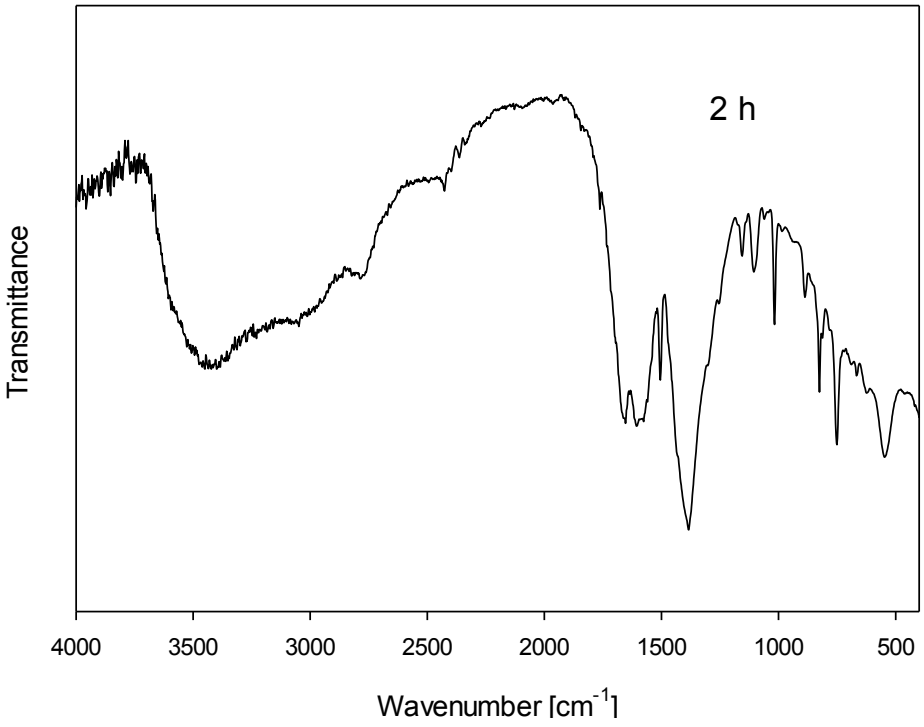
2 h
Transmittance
4000
3500
3000
2500
2000
1500
1000
500
Wavenumber [cm-1]

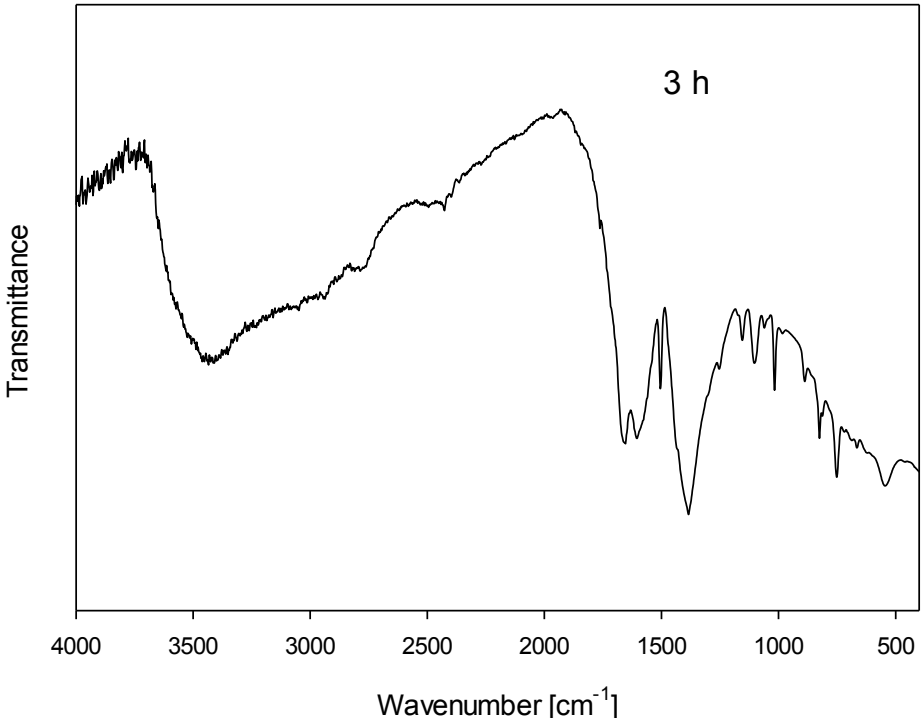
3 h
Transmittance
4000
3500
3000
2500
2000
1500
1000
500
Wavenumber [cm-1]

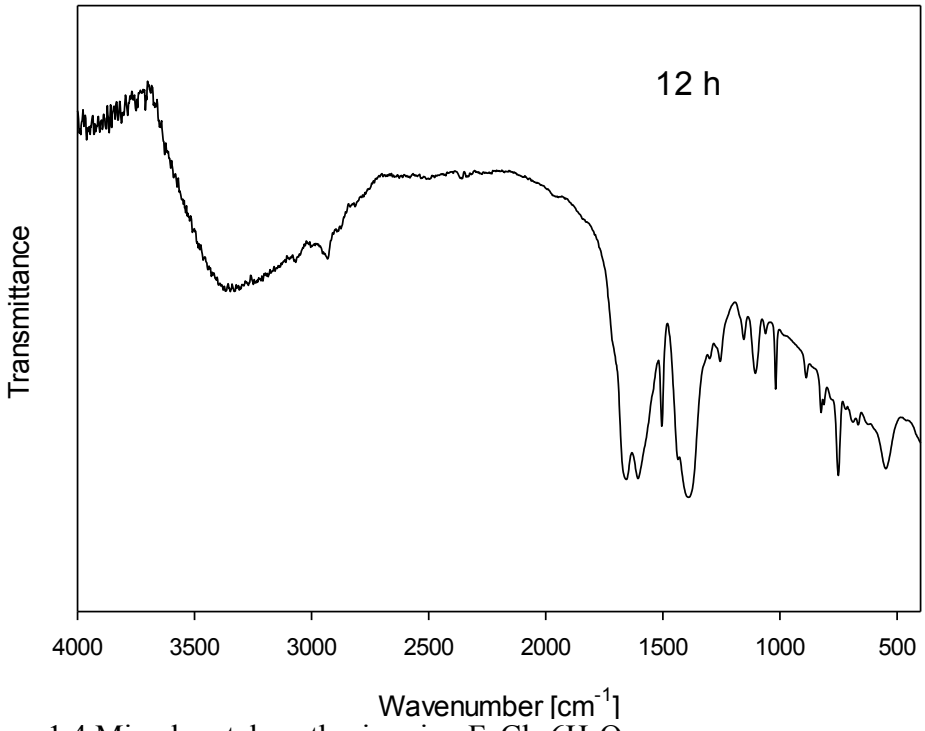

1.4.Mixed metal synthesis using $FeCl_3.6H_2O$

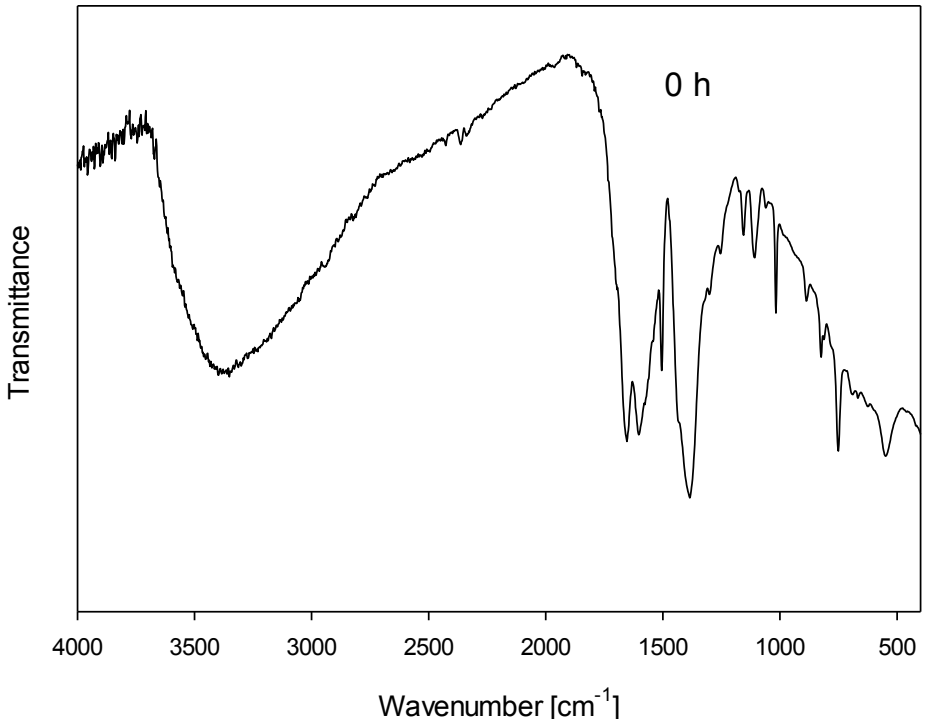

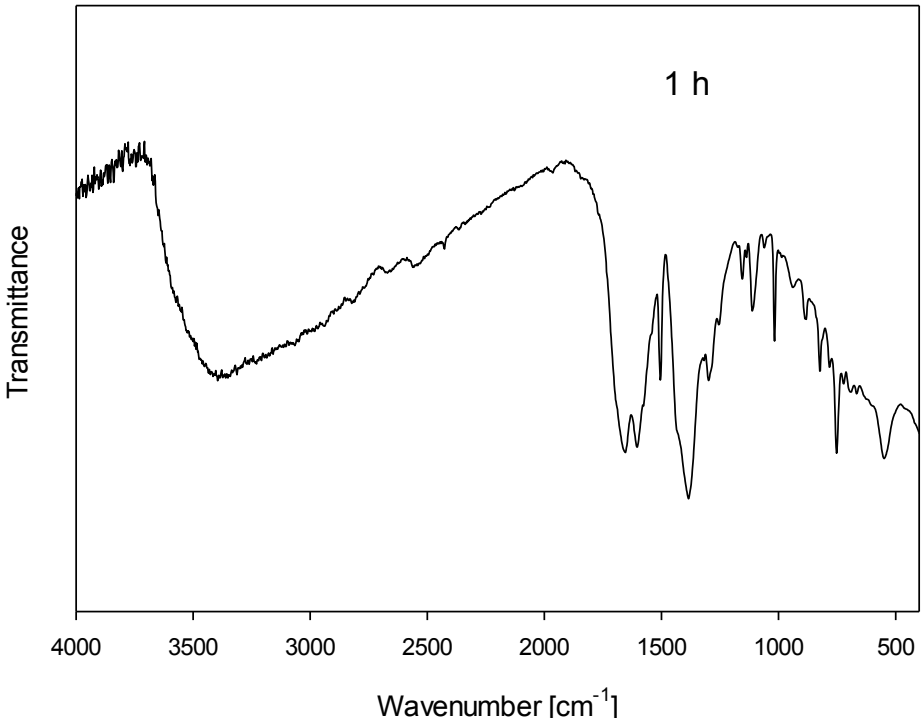
1 h
Transmittance
4000
3500
3000
2500
2000
1500
1000
500
Wavenumber [cm-1]

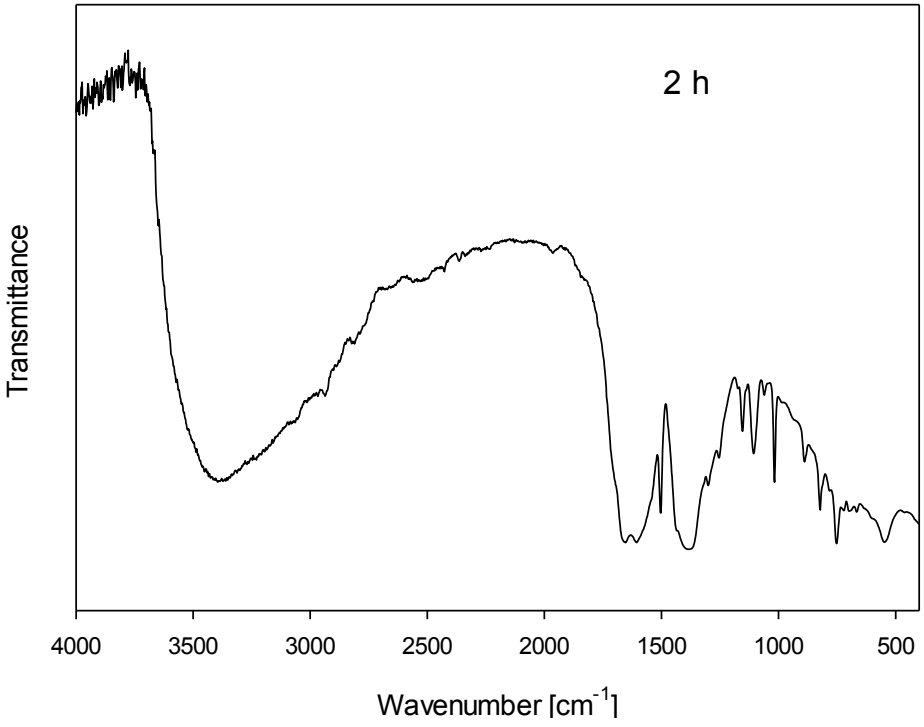
2 h
Transmittance
4000
3500
3000
2500
2000
1500
1000
500
Wavenumber [cm-1]

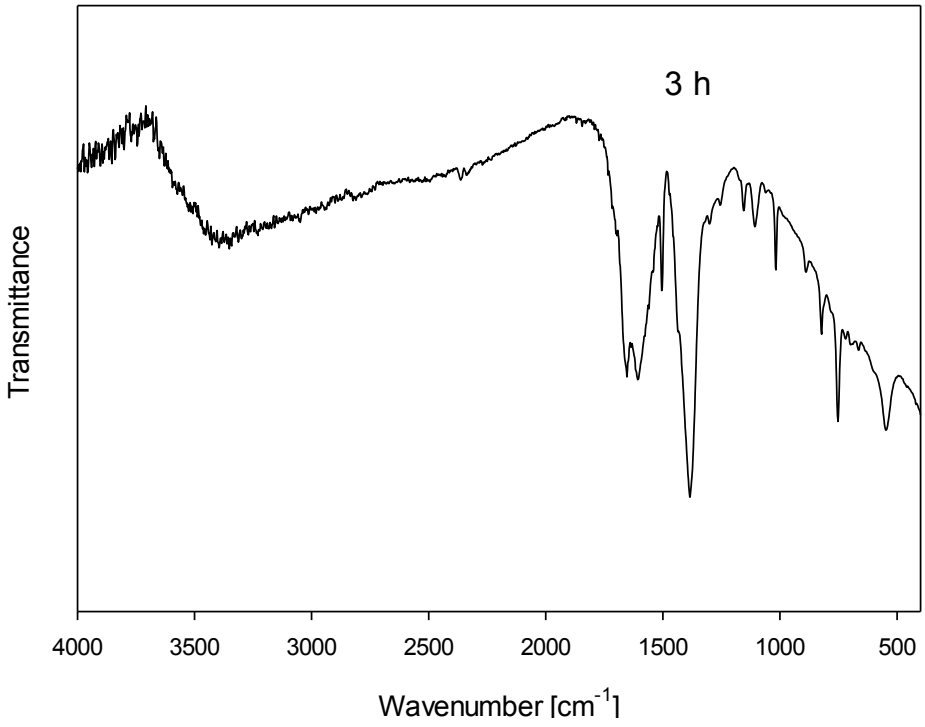
3 h
Transmittance
4000
3500
3000
2500
2000
1500
1000
500
Wavenumber [cm-1]

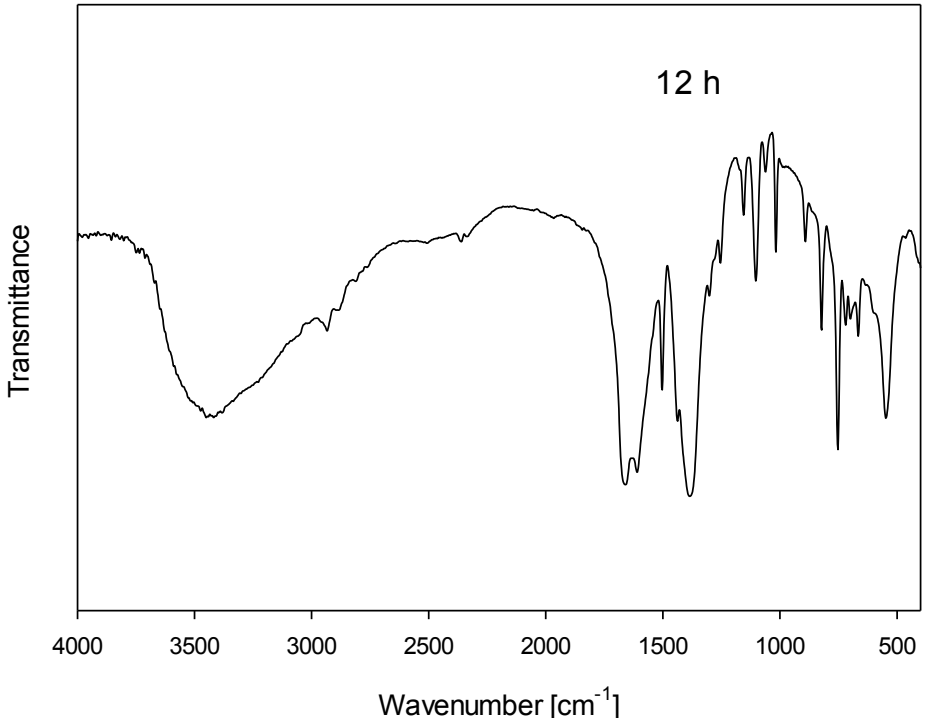
12 h
Transmittance
4000
3500
3000
2500
2000
1500
1000
500
Wavenumber [cm-1]

2. HRTEM and EDS analysis

EDS spectra of 5 positions taken on the same Fe_2Ni-MIL-88B crystal (see Figure 9 in the article).

Since the samples were dispersed on a copper grid for analysis. Signal of copper was observed in the EDS spectra.

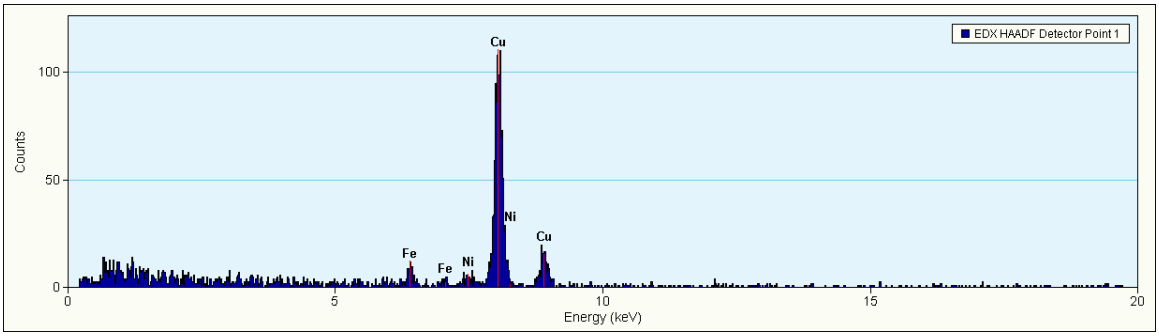

EDS spectroscopy of position 1

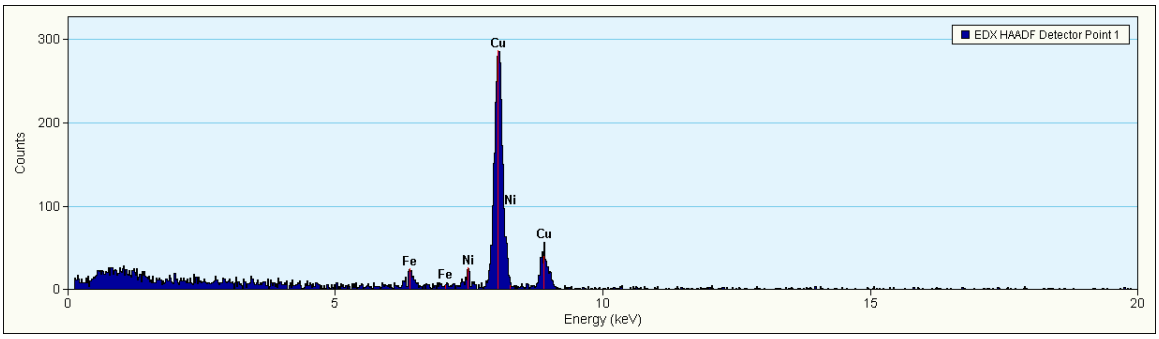

EDS spectroscopy of position 2

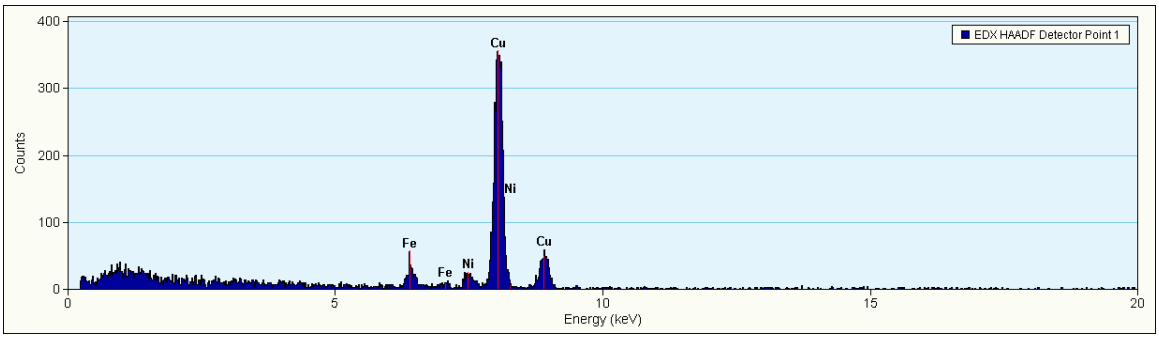

EDS spectroscopy of position 3

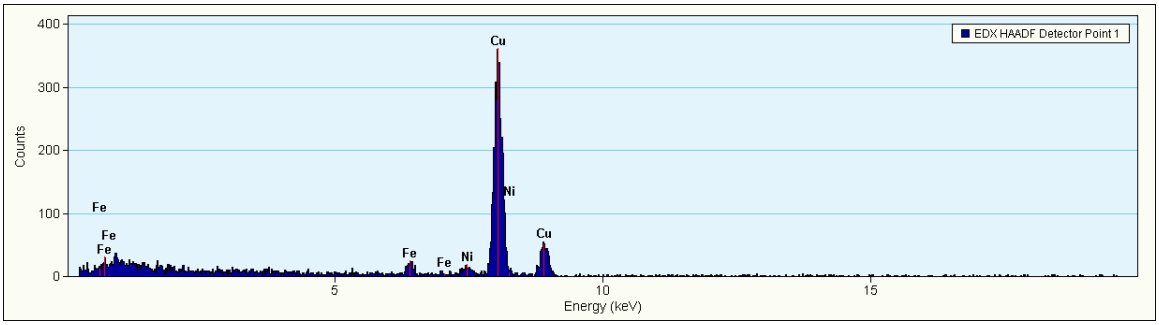

EDS spectroscopy of position 4

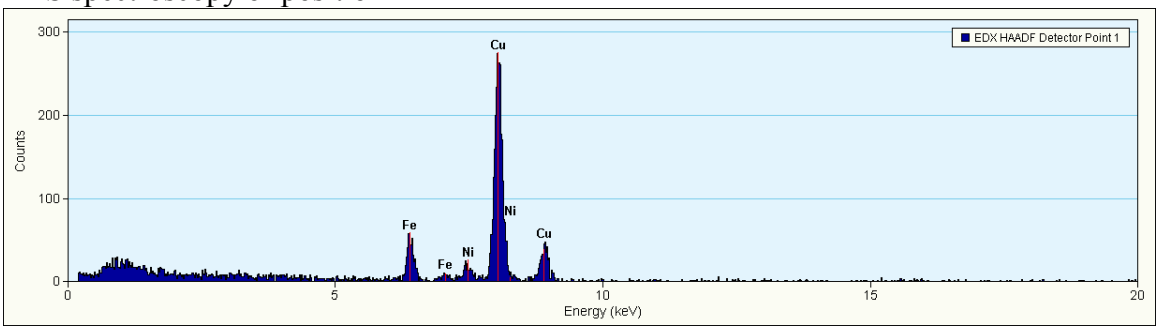

EDS spectroscopy of position 5

3. XPS analysis of Fe_2Ni-MIL-88B-12h, dried

The X-ray photoelectron spectra (XPS) were taken on a photoelectron spectrometer (KRATOS AXIS-ULTRA) with a monochromatic X-ray source of Al Kα . The operating conditions for recording high-resolution spectra were as follows: 1486.6 eV and 225 W; pass energy of 160 eV with anoperating pressure of 10^{-9} Torr.

CasaXPS software was use to analys the collected XPS spectra. [1] All spectra were calibrated using the adventitious C 1s peak with a fixed value of 284.8 eV. Shirley background was then applied and subtracted.

As the Fe cation in trinuclear cluster is at high spin state,[2,3] envelope of Fe $2p_{3/2}$ spectrum was fit with peaks corresponding to the GS multiplets, surface structures and shake-up-related satellites.[4-6] All the four GS multiplets have the same full width at half-maximum (FWHM) of 1.6 eV and their peak areas are in similar to those of multiplets. The rest of the envelop was filled with one surface structure peak and one satellites peak.

Fitting result is in agreement with Fe^{3+} GS multiplets , suggesting the presence of only Fe^{3+} not Fe^{2+} in the sample.

Gupta and Sen (GS) multiplet peak parameters used to fit the high-spin Fe^{3+}

Sample	Peak 1			Peak 2			Peak 3			Peak 4		
	eV	% area	ΔE	eV	% area	ΔE (eV)	eV	% area	ΔE (eV)	eV	% area	ΔE (eV)
Fe_2Ni-MIL-88B-12h	713.2	7	1.3	711.9	21	1.1	710.8	35	1.5	709.3	37	
GS Fe3+ multiplets		10	0.6		20	1.3		30	1.6		40	

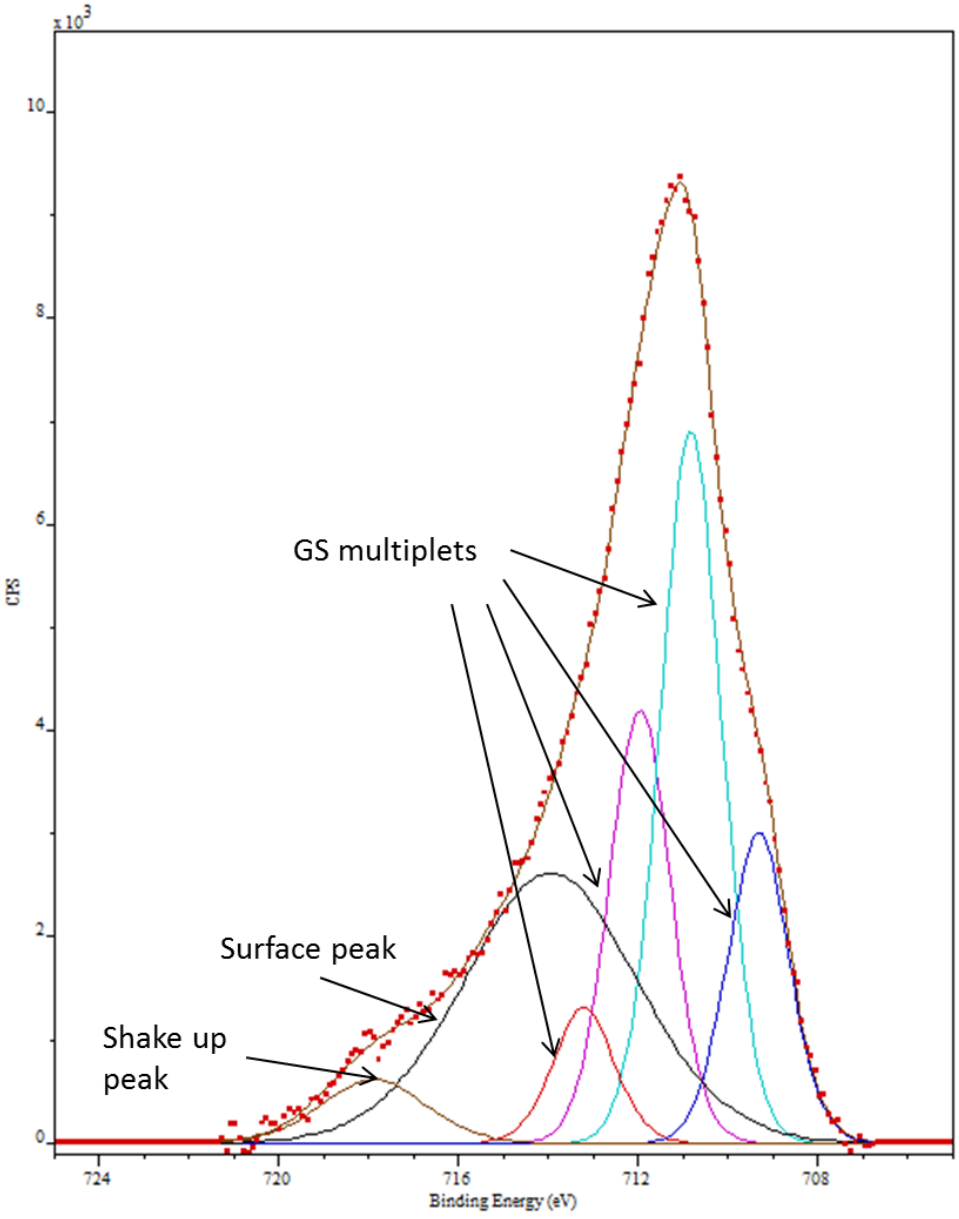

References

1. Fairley N. CasaXPS Version 2.2.19, copyright 1999–2003
2. Boudalis A. K. et al *Polyhedron* **2005**, *24*, 1540
3. Psycharis, V et al *Eur. J. Inorg. Chem* **2006**, *2006*, 3710-
4. Gupta RP, Sen SK. *Phys. Rev. B.* **1975**; *12*: 15
5. Grosvenor A.P et al. *Surf. Interface Anal*. **2004**, *36,* 1564
6. Mullet M. et al. *Surf. Interface Anal*. **2008**, *40*, 323